Mrx6 regulates mitochondrial DNA copy number in *S. cerevisiae* by engaging the evolutionarily conserved Lon protease Pim1

Aylin Göke[1], Simon Schrott[3], Arda Mizrak[2], Vladislav Belyy[1], Christof Osman[1,3,*] and Peter Walter[1,*]

[1] Howard Hughes Medical Institute and Department of Biochemistry and Biophysics, University of California at San Francisco, San Francisco, USA

[2] Department of Physiology, University of California at San Francisco, San Francisco, USA

[3] current address: Department of Biology II, Biozentrum of the Ludwig-Maximilian-Universität, Munich, Germany

[*] Corresponding Authors: peter@walterlab.ucsf.edu

osman@biologie.uni-muenchen.de

Key words:

mtDNA, mtDNA copy number, mtDNA copy number control, mtDNA maintenance, nucleoids, Lon protease, PET20 domain, Pim1, Mrx6, mitochondria, *S. cerevisiae*

Abstract

Mitochondrial function crucially depends on the maintenance of multiple mitochondrial DNA (mtDNA) copies. Surprisingly, the cellular mechanisms regulating mtDNA copy number remain poorly understood. Through a systematic high-throughput approach in *S. cerevisiae,* we determined mtDNA to nuclear DNA ratios in 5148 strains lacking non-essential genes. The screen revealed *MRX6,* a largely uncharacterized gene, whose deletion displayed a marked increase of mtDNA levels, while maintaining WT-like mitochondrial structure and cell size. Quantitative super-resolution imaging revealed that deletion of *MRX6* alters both the size and spatial distribution of mtDNA nucleoids. We demonstrate that Mrx6 partially colocalizes with mtDNA within mitochondria and interacts with the conserved Lon protease Pim1 in a complex that also includes Mam33 and the Mrx6-related protein Pet20. Acute depletion of Pim1 phenocopied the high mtDNA levels observed in Δ*mrx6* cells. No further increase of mtDNA copy number was observed upon depletion of Pim1 in Δ*mrx6* cells, revealing an epistatic relationship between Pim1 and Mrx6. Human and bacterial Lon proteases regulate DNA replication by degrading replication initiation factors, suggesting a model in which Pim1 acts similarly with the Mrx6 complex providing a scaffold linking it to mtDNA.

Introduction

Mitochondria are endosymbiotic organelles that carry multiple copies of their own genome, encoding proteins required for oxidative phosphorylation and respiratory metabolism. mtDNA copies are packaged together with several mtDNA binding proteins to form nucleoids that distribute throughout the mitochondrial network and display a semi-regular spacing in the mitochondrial network (Chen and Butow, 2005; Brown *et al.*, 2011; Osman *et al.*, 2015; Jajoo *et al.*, 2016; Lewis *et al.*, 2016). The copy number of mtDNA in each cell is maintained within a narrow range (Chen and Butow, 2005; Clay Montier *et al.*, 2009). Previous studies reported that *S. cerevisiae* cells maintain ~40-60 nucleoids, each carrying ~1-2 mtDNA copies (Chen and Butow, 2005), although some reviews cite up to 10 copies per nucleoid (Lipinski *et al.*, 2010). Mammalian cells can contain thousands of nucleoids depending on tissue type (Williams, 1986; Miller *et al.*, 2003). Recent super resolution microscopy experiments demonstrated that most nucleoids contain only a single mtDNA copy (Kukat *et al.*, 2011).

Altered levels of mtDNA are linked to a variety of diseases, including neurodegenerative and metabolic diseases and various types of cancer (Liu *et al.*, 2006; Clay Montier *et al.*, 2009; Ylikallio *et al.*, 2010; Yu, 2011; Kornblum *et al.*, 2013; Mengel-From *et al.*, 2014; Pyle *et al.*, 2016). Furthermore, increasing mtDNA copy number has been suggested to help cells to ameliorate the effect of myocardial infarction in mice (Ikeda *et al.*, 2015). Despite their physiological importance, the cellular mechanisms that regulate mtDNA copy number remain poorly understood. Previous genetic screens designed to identify new components that control mtDNA copy number focused on mutants that lead to mtDNA loss and identified numerous components important for mtDNA maintenance (Fukuoh *et al.*, 2014; Zhang and Singh, 2014). However, loss of mtDNA is often caused by secondary effects due to

compromised mitochondrial function (Lipinski *et al.*, 2010). Therefore, the question of how mtDNA copy number is regulated to remain within a narrow window has remained largely unanswered.

To elucidate how mtDNA levels are sustained at their physiological set-point, we determined mtDNA levels in a yeast deletion library. This screen revealed the gene *MRX6* as a crucial component of mtDNA copy number control.

Results

A genetic screen identifies cellular machineries regulating mtDNA copy number

We systematically determined the amount of mtDNA relative to nuclear DNA (nDNA), in 5148 strains of a yeast gene-deletion library generated in S288c cells, each lacking a different non-essential gene (*Saccharomyces* Genome Deletion Project) (Giaever *et al.*, 2002). Mutant colonies grown on rich medium were transferred to nylon membranes, lysed, and hybridized with two different sets of fluorescent probes, specific for mtDNA and nDNA respectively (Figs. 1A and B). We determined the fluorescent intensity of both probes and calculated the mtDNA/nDNA ratio for each mutant. Mutants were classified into three categories: 1) mutants that contained an increased mtDNA/nDNA ratio, 2) mutants that maintained their mtDNA/nDNA ratio similar to wild-type cells (WT), and 3) mutants that lost the majority or all of mtDNA (Fig. 1C) (Supp. Fig. 1A; Supp. Table 1). The following observations indicate that this screen faithfully reports on mtDNA levels: ~80% of mutants falling into the third category were previously described to be respiratory-deficient or defective in maintenance of mtDNA (Supp. Fig. 1B; Supp. Table 1B). Furthermore, mutants lacking the genes *SML1, RRM3* and

86 *RFX1*, which were previously reported to contain elevated levels of mtDNA (Taylor *et al.*,
87 2005), were also identified with increased mtDNA/nDNA ratios in our analysis (Supp. Table
88 1A).

89 Loss or reduction of mtDNA can result in various mitochondrial defects (Lipinski *et al.*,
90 2010). Therefore, we focused on mutants that displayed higher mtDNA/nDNA ratios, which is
91 more likely to be indicative of a defect in mDNA copy number regulation. To validate our hits,
92 we repeated the colony blot hybridization with the initially identified candidates (167 mutants)
93 and selected 91 mutants, for which increased mtDNA levels were reproduced, for further
94 analysis (Supp. Fig. 1C; Supp. Table 1C). As yeast colonies on agar plates consist of
95 heterogeneous cell populations that differ in metabolic and respiratory states (Traven *et al.*,
96 2012), we isolated genomic DNA from the 91 mutants grown in liquid cultures from early-mid
97 logarithmic phase and quantified their mtDNA levels relative to WT cells by quantitative PCR
98 (qPCR). A majority of the mutants (73 of 91) showed a >50% increase in the mtDNA/nDNA
99 ratio (Supp. Table 1D).

100 In yeast, mtDNA copy number linearly correlates with the length of the mitochondrial
101 network (Osman *et al.*, 2015). Furthermore, mitochondrial network volume correlates linearly
102 with cell volume (Rafelski *et al.*, 2012). For this reason, elevated mtDNA levels could result as
103 a secondary effect of increased cell size, as would be expected, for example, in mutants that
104 affect cell cycle progression (Conrad and Newlon, 1982). To eliminate such mutants from our
105 analyses, we determined the cell size of the 91 candidates by flow-cytometry using side-
106 scattered light as a proxy. Indeed, a majority of the mutants showed an increase in cell size (Fig.
107 1D; Supp. Table 1D). By contrast, nine mutants displayed cell sizes that were within 10% of the
108 value obtained for WT cells, making them likely candidates involved in mtDNA copy number

regulation (Fig. 1E).

Deletion of *MRX6,* a largely uncharacterized gene, increases mtDNA copy number

From the genes whose deletion resulted in increased mtDNA levels without altering cell size, we chose to focus on *MRX6* because: 1) the mtDNA/nDNA ratio increase in Δ*mrx6* cells was the highest among the mutants that do not affect cell size (Fig. 1D), 2) Mrx6 has a predicted mitochondrial targeting sequence, and 3) Mrx6 belongs to an uncharacterized protein family. To verify that increased levels of mtDNA were linked to deletion of *MRX6* and not caused by second-site mutations in the library strain, we engineered a fresh Δ*mrx6* deletion strain, which reproduced the phenotype of strongly elevated mtDNA levels (Fig. 2A). While we observed a ~2.5-fold increase in the library strain, we observed only a ~1.5-fold increase in the newly generated strain. We attribute this difference to the fact that the strains were generated in different yeast backgrounds (S288c vs. W303), carrying different amounts of mtDNA (Connelly and Akey, 2012), and/or to a possibility of aggravating second site mutations in the deletion library strain. The 1.5-fold increase in Δ*mrx6* cells versus WT cells was statistically significant ($p<0.01$). For the remaining experiments, we used the freshly generated Δ*mrx6* W303 strain.

Previous studies reported that mtDNA abundance ranges from 25 to 100 copies per cell depending on the strain and growth conditions (MacAlpine *et al.*, 2000; Chen and Butow, 2005). To obtain an accurate quantification of mtDNA levels in our strains, we determined the absolute mtDNA copy number by qPCR analysis using oligonucleotides specific for nuclearly encoded *ACT1* and mitochondrially encoded *COX1*. To this end, we cloned ~1 kb fragments of *ACT1* and *COX1* into plasmids, which we used as standards to correlate threshold PCR cycle

values to copy number. According to these measurements, we conclude that haploid WT cells have 21 (± 4) copies of mtDNA, whereas Δ*mrx6* cells carry 32 (± 5) copies (Fig. 2A).

We next tested whether deletion of *MRX6* compromises mitochondrial function. To this end, we monitored growth of Δ*mrx6* cells on a non-fermentable carbon source, which necessitates a functional respiratory chain. Δ*mrx6* cells did not exhibit any growth phenotype compared to WT cells (Fig. 2B). Next, we tested mtDNA levels in WT and Δ*mrx6* cells grown under different conditions, such as i) a non-fermentable carbon source, ii) under oxidizing stress, and iii) in presence of an electron transport chain uncoupler (Figs. 2C and D). These analyses revealed that absence of *MRX6* leads to a robust increase of mtDNA under all conditions tested and that it occurs independent of metabolic or stress adaption responses.

As deletion of *MRX6 increased* mtDNA levels, we next asked whether over-expression of Mrx6 would *decrease* them. We over-expressed a C-terminally myc-tagged version of Mrx6 (Mrx6-myc) (Supp. Fig. 2), but did not observe altered mtDNA levels (Figs. 2E and F). Mrx6-myc was functional because it maintained mtDNA at WT levels when it was expressed as the only copy of the gene. Taken together, deletion of *MRX6* increases mtDNA copy number without compromising mitochondrial function, while conversely over-expression of Mrx6 does not affect mtDNA levels.

Deletion of *MRX6* increases mtDNA copy number without altering mitochondrial network length or morphology

To test whether deletion of *MRX6* causes abnormalities in mitochondrial volume or morphology, we visualized the mitochondrial network with a mitochondria-targeted red fluorescent protein (mt-dsRed) in Δ*mrx6* and WT cells by fluorescence microscopy (Fig. 3A).

We did not detect any changes in mitochondrial morphology (Figs. 3B and C) or network length (Fig. 3D) in Δ*mrx6* cells, demonstrating that elevated mtDNA levels in Δ*mrx6* cells were not a consequence of morphological alterations.

To determine copy number of mtDNA in single cells, we used our recently developed mt-LacO-LacI system to visualize mtDNA by fluorescence microscopy. The system is based on an array of LacO repeats integrated into mtDNA, which can be bound by a mitochondria-targeted GFP-tagged LacI protein (Osman *et al.*, 2015). In contrast to our previous work, we applied structured illumination (SI) microscopy on fixed diploid cells to resolve mtDNA copies that are in close proximity to one another (Fig. 3A). We counted ~28 mtDNA copies in WT diploid cells, which is in good agreement with 33 (± 6) mtDNA copies determined by qPCR (Fig. 2A), indicating that the microscopic analysis resolved single mtDNA copies in the majority of cases for WT cells. Given that cells used in this experiment were not synchronized and were going through different stages of cell cycle, resulting in differences in cell size and mitochondrial volume, we compared mtDNA copy number normalized to mitochondrial network length. Deletion of *MRX6* increased the number of mtDNA copies normalized to mitochondrial network length by 1.3-fold (Fig. 3E; WT=1.16, Δ*mrx6*=1.54 mtDNA copies/µm network length). Of note, a 1.3-fold increase is smaller than what we obtained with qPCR (Fig. 2A). We attribute the difference between microscopy and qPCR analysis to the fact that even with SI microscopy, we did not resolve mtDNA copies that were close to one another (such as replicating mtDNA copies).

Next, we compared the distances between mtDNA copies in the three-dimensional mitochondrial network. Consistent with the increased number of nucleoids within the same length of mitochondrial network, the mean distances between mtDNA copies were 692 nm and

872 nm for Δ*mrx6* and WT cells, respectively ($p<0.001$; Fig. 3F). However, upon more detailed examination, we found that this difference was largely due to a closer apposition of a subset of mtDNA copies in the smaller distance range, while mtDNA copies further apart maintained their distribution as in WT cells. This bias is quantified in Figure 3G, which shows that mtDNA distances in the 0.5 to 1.0 µm range were disenriched in the mutant cells as compared to WT cells (Fig. 3G, blue box), whereas mtDNA distances below 0.5 µm were enriched (Fig. 3G, yellow box). These nonlinear alterations in the placement of mtDNA copies to each other in Δ*mrx6* cells are in line with the observation that the overall mitochondrial network length is not altered in the mutant.

We next stained fixed diploid cells with DAPI and analyzed them by SI microscopy (Fig. 4A). In contrast to the LacO/LacI system shown above, DAPI stains mtDNA in its entirety rather than just demarking a single locus on it. DAPI staining in WT cells revealed distinct punctate structures known as nucleoids (Meeusen and Nunnari, 2003). While Δ*mrx6* cells showed the same number of nucleoids, the average volume of nucleoids was enlarged ~2.2-fold compared to WT cells (Figs. 4B and C). We verified this finding by using an anti-DNA antibody (Supp. Fig. 3) to ascertain that it was indeed DNA and not other DAPI-stained macromolecules, such as RNA, that gave rise to the increased volume. Notably, nucleoids in Δ*mrx6* cells displayed an oblong shape: their lengths when traced along the mitochondrial network were significantly increased (mean length of nucleoids were 630 nm and 430 nm for Δ*mrx6* and WT cells, respectively; $p<0.001$; Supp. Figs. 3A and 3B). Taken together these data show that deletion of *MRX6* increases mtDNA copy number without affecting mitochondrial network length or shape, but alters the spatial organization and shape of nucleoids.

Mrx6 is a member of the PET20 domain-containing protein family

Interestingly, inspection of the Mrx6 sequence revealed the presence of a PET20 domain of uncharacterized structure and function, which in *S. cerevisiae* is found in two other mitochondrial proteins, Sue1 and Pet20 (Fig. 5A). In addition to the PET20 domain, Mrx6 has a unique C-terminal extension that distinguishes it from the rest of the PET20 domain-containing proteins (Supp. Fig. 4). To assess whether other PET20 domain-containing proteins are important for maintaining mtDNA levels, we deleted the genes encoding these proteins in different combinations and quantified the change of mtDNA levels by qPCR. In line with the colony blots from the initial screen, single deletions of *PET20* or *SUE1* did not alter mtDNA levels significantly. Additionally, no further increase in mtDNA levels compared to Δ*mrx6* cells was observed in Δ*mrx6* Δ*pet20*, Δ*mrx6* Δ*sue1,* and Δ*mrx6* Δ*pet20* Δ*sue1* double and triple mutant strains (Fig. 5B). Thus, neither maintenance of normal mtDNA levels nor increase in mtDNA levels in Δ*mrx6* cells requires Pet20 or Sue1.

Mrx6 forms foci in mitochondria and colocalizes with mtDNA

Mrx6 has a predicted mitochondrial targeting sequence, but to date its localization has not been experimentally determined. We constructed a yeast strain in which we genomically tagged Mrx6 in its endogenous locus with the fluorescent protein mNeonGreen (Mrx6-Neon) to determine its localization by fluorescence microscopy. Cells expressing Mrx6-Neon displayed mtDNA levels indistinguishable from WT cells, indicating that protein function was preserved in the tagged Mrx6 variant (Supp. Fig. 5A). In agreement with its predicted mitochondrial localization, Mrx6-Neon colocalized with mitochondrial matrix-targeted blue fluorescent protein (mtTagBFP) (Fig. 6A). Interestingly and by contrast to mtTagBFP, Mrx6-Neon formed

219 discrete punctate structures that were non-uniformly distributed along the mitochondrial
220 network.

221 The punctate localization of Mrx6-Neon was reminiscent of the distribution of mtDNA
222 in the nucleoids in the mitochondrial network. Thus, we next tested whether Mrx6-Neon
223 colocalizes with mtDNA. We stained Mrx6-Neon expressing cells with DAPI and determined
224 Mrx6-Neon and mtDNA localization. These analyses revealed that a fraction of Mrx6-Neon
225 puncta colocalized with the DAPI signal (Fig. 6B; arrow), whereas others did not (Fig. 6B;
226 asterisk). We quantitatively assessed the proportion of the Mrx6-Neon signal that colocalized
227 with DAPI and *vice versa* by determining the Manders' colocalization coefficient (MCC)
228 between intensity profiles of both fluorescent signals along the mitochondrial network (Figs. 6C
229 and Supp. 5B). The MCC values showed a broad distribution, yet the majority of cells showed
230 ~60% overlap between the two wavelengths, confirming our initial observation of a partial
231 colocalization between Mrx6 and mtDNA (Fig. 6D). Pearson's Correlation Coefficient (PCC)
232 analysis further supported colocalization (Fig. 6E). To validate these conclusions, we evaluated
233 the significance of the measured MCC and PCC values by comparing our results to a control
234 dataset. This dataset consisted of the same intensity profiles, in which one of the two color
235 channels was randomized (Supp. Fig. 5C). The control MCC and PCC values were consistently
236 lower and showed a significantly different distribution compared to the measured data (Figs.
237 6D, 6E and Supp. 5D; $p<0.001$). Additionally, comparing the measured MCC and PCC values
238 to a simulated data set in which one of the two channels was shifted against the respective other
239 channel, rather than randomized, further validated these results.

240 Given that only ~60% of the Mrx6-Neon puncta colocalized with nucleoids, we asked
241 whether Mrx6 might still forms punctate structures in the absence of mtDNA. Mrx6-Neon was

still observed in puncta in mitochondria of mtDNA lacking cells (rho^0) (Fig. 6F). Taken together, Mrx6 localizes to mitochondria and forms puncta that distribute throughout the mitochondrial matrix and partially colocalize with mtDNA. However, the presence of mtDNA is not necessary for the formation of Mrx6 puncta.

Mrx6 forms a complex with Pet20, Mam33 and Pim1

Next, we aimed to identify interaction partners of Mrx6 to begin getting a molecular understanding about how Mrx6 affects mtDNA levels. To this end, we immunoprecipitated functional C-terminally Flag-tagged Mrx6 (Mrx6-Flag, Supp. Fig. 6) and identified interacting proteins by mass spectrometry (MS). The proteins Pim1, Mam33 and, to our surprise, Pet20, co-purified with Mrx6-Flag but were absent in the eluate fraction of control immunoprecipitations from cells that only expressed untagged Mrx6 (Figs. 7A and B).

Pim1 is a highly conserved ATP-dependent mitochondrial Lon protease (Venkatesh *et al.*, 2012), and Mam33 is a specific translational activator of Cox1 mRNA (Roloff and Henry, 2015). We next asked whether, reciprocally, we could co-purify these components by pulling down C-terminally Flag-tagged Pet20 (Pet20-Flag). Strikingly, Mrx6, Pim1 and Mam33 co-purified with Pet20-Flag, thus revealing an interaction network between these four proteins (Fig. 7C). We further examined the interaction hierarchy between these proteins by pulling down Mrx6-Flag from extracts of Δ*pet20* cells. The results showed that Pet20 was dispensable for the interaction between Mrx6-Pim1 and Mrx6-Mam33 (Fig. 7B). By contrast, upon Pet20-Flag pull-down from Δ*mrx6* lysates, Pim1-Pet20 and Mam33-Pet20 interactions were drastically reduced or not detected, respectively, suggesting that Mrx6 bridges Pim1, Mam33, and Pet20 (Fig. 7C).

Since two proteins of the PET20 domain protein family, Mrx6 and Pet20, are found in a protein interaction network together with Pim1 and Mam33, we asked whether the third member of the PET20 domain protein family, Sue1, would show a similar protein interaction profile. To this end, we immunoprecipitated C-terminally Flag-tagged Sue1 (Sue1-Flag). In agreement with the Mrx6-Flag and Pet20-Flag pull-downs that did not identify Sue1, neither Mrx6 nor Pet20 co-immunoprecipitated with Sue1-Flag. However, this experiment revealed that Pim1 also interacts with Sue1 (Fig. 7D). Thus, Pim1 is a common interaction partner of all three PET20 domain-containing proteins.

Taken together, these results show that Mrx6, Pet20, Pim1 and Mam33 are part of a physical interaction network in which Mrx6 is crucial for the complex's architecture, whereas Pet20 is dispensable. In addition, our results support the conclusion that Sue1 forms a separate complex with Pim1, which does not include Mrx6 or Pet20.

Mrx6 partially colocalizes with Pet20 and Pim1

As Mrx6 and Pet20 are part of an interaction network, we next examined the spatial association between them in single cells. To this end, we engineered a yeast strain expressing Mrx6-Neon and C-terminally mRuby-tagged Pet20 (Pet20-Ruby) and performed live-cell microscopy.

Pet20-Ruby showed discrete punctate structures along the mitochondrial network similar to Mrx6 (Fig. 8A). Surprisingly, we observed only partial colocalization between Mrx6 and Pet20, in which only some of Mrx6-Neon puncta colocalized with Pet20-Ruby (Fig. 8A; arrow), and *vice versa*. MCC values showed ~50% overlap between Mrx6-Neon and Pet20-Ruby signals (Figs. 8B and Supp. 7A; $p<0.001$), and PCC analysis confirmed their colocalization (Fig. 8C; $p<0.001$).

We next tested whether Mrx6 would display a similar, partial colocalization with Pim1, a notion suggested by our finding that Pim1 forms a separate complex with Sue1 that lacks Mrx6 or Pet20 (Fig. 7D). Hence, we analyzed the association between Mrx6 and Pim1 using a yeast strain expressing Mrx6-Neon and C-terminally mRuby-tagged Pim1 (Pim1-Ruby), which preserves protein function (Supp. Fig. 7B). We observed partial colocalization between Mrx6 and Pim1 (Fig. 8D). MCC values showed ~50% overlap between Mrx6-Neon and Pim1-Ruby signals (Figs. 8E and Supp. 7C; $p<0.001$), and PCC analysis further supported their colocalization (Fig. 8F; $p<0.001$). Taken together, these data indicate that Mrx6, partially colocalizes with Pet20 and Pim1, suggesting that they form sub-complexes along the mitochondrial network.

The Mrx6 complex colocalizes with mtDNA

We next tested whether colocalization of Mrx6 with Pet20 and Pim1 may preferentially occur in regions close to mtDNA. To this end, we performed triple labeling experiments in which we stained mtDNA with DAPI in cells expressing Mrx6-Neon and Pet20-Ruby. This experiment revealed instances of colocalization between Mrx6-Neon, Pet20-Ruby and mtDNA (Fig. 9A). The complexity of images displaying three colors in the confined space of mitochondria necessitated a careful quantification of the degree of colocalization. To this end, we binned regions of the Mrx6-Neon and Pet20-Ruby intensity profiles where (1) both proteins colocalized, (2) only Mrx6-Neon but no Pet20-Ruby localized, and (3) only Pet20-Ruby but no Mrx6-Neon localized. We then asked, whether these regions would differentially colocalize with mtDNA. Determination of the MCC values revealed that in Bin1 (Mrx6-Pet20) on average 77% of the regions colocalized with DAPI (Figs. 9B and Supp. 8A). By contrast, in Bin 2 (Mrx6 alone) or Bin 3 (Pet20 alone) only 56% or 42% of the regions, respectively, colocalized

with DAPI, which was significantly different from Bin 1 ($p<0.001$; Fig. 9B and Supp. Fig. 8A). As a control, we generated a dataset by randomizing the DAPI intensity profile against the Mrx6 and Pet20 profiles and re-calculated the MCC values. Strikingly, the proportion of the Mrx6-Pet20 signal colocalizing with the DAPI signal was reduced to 44% (Figs. 9C and Supp. 8B), matching the colocalization with mtDNA observed for Mrx6 alone (45%; Bin 1 - Bin 2 $p=0.78$; Fig. 9C) or Pet20 alone (44%; Bin 1 – Bin 3 $p=0.79$; Supp. Fig. 8B). These results suggest that Mrx6-Pet20 colocalization preferentially occurs in regions close to mtDNA rather than areas that are devoid of mtDNA.

In an analogous set of experiments, we examined the colocalization between Mrx6-Neon, Pim1-Ruby and mtDNA (Fig. 9D). The MCC values revealed that on average 65% of the areas, in which Mrx6-Neon and Pim1-Ruby were found together, colocalized with the DAPI signal (Figs. 9E and Supp. 8C); whereas only 46% of the Mrx6 signal ($p<0.001$; Fig. 9E), and 36% of the Pim1 signal colocalized with the DAPI signal when they were alone ($p<0.001$; Supp. Fig. 8C). Moreover, the percentage of the Mrx6-Pim1 signal colocalizing with the randomized DAPI signal reduced to 38% (Figs. 9F and Supp. 8D), closely matching the values for Mrx6 alone (37%; $p=0.49$; Fig. 9F) and Pim1 alone (38%; $p=0.29$; Supp. Fig. 8D). These data indicate that similar to Mrx6-Pet20, Mrx6-Pim1 colocalization also occurs in areas close to mtDNA. Taken together, our data suggest that Mrx6 associated with Pet20 or Pim1 preferentially colocalizes with mtDNA, whereas the individual components —or yet to be defined partially assembled subcomplexes— are mostly found in the areas devoid of mtDNA.

Depletion of Pim1 increases mtDNA levels

Our biochemical and microscopic analyses suggest that Mrx6 may determine mtDNA levels via its interaction with Pim1. To test this model, we examined mtDNA levels in cells

over-expressing or lacking Pim1 by qPCR. Over-expression of Pim1 in WT and Δ*mrx6* cells reduced mtDNA copy number (Supp. Fig. 10A), supporting a putative role of Mrx6 as a regulatory component conferring substrate specificity to Pim1. However, when *PIM1* was deleted, mtDNA copy numbers varied widely in different Δ*pim1* and Δ*pim1*Δ*mrx6* clones, preventing an unequivocal interpretation (Supp. Fig. 10B). These inconsistent results are likely explained by the dysregulated accumulation of the many Pim1 substrates (Major *et al.*, 2006; Bayot *et al.*, 2010), leading pleiotropically to mitochondrial dysfunction.

To mitigate such pleiotropic effects, we integrated a construct facilitating estradiol-dependent expression of Pim1 into WT yeast strains and subsequently generated endogenous deletions of either *PIM1* (Δ*pim1 Pestr-PIM1*) or *MRX6* and *PIM1* (Δ*mrx6* Δ*pim1 Pestr-PIM1*). Pim1 expression was maintained throughout strain generation by growing cells in the presence of estradiol. Estradiol concentrations of 25 nM were sufficient to restore respiratory growth in Δ*pim1* background at the experimental conditions at 30 °C (Fig. 10C), and also resulted in low expression levels that allowed fast Pim1-depletion upon estradiol removal (Fig. 10B).

We acutely depleted Pim1 by shifting cells to medium lacking estradiol and determined mtDNA levels over the time course of 20 hours (Figs. 10A and 10B). In line with the low expression level of Pim1 at the start of the experiment, mtDNA levels were increased ~1.3-fold in Δ*pim1 Pestr-PIM1* cells compared to WT. When Pim1 was depleted, 12 hours after removal of estradiol, mtDNA levels were increased 1.8-fold in Δ*pim1 Pestr-PIM1* cells (Fig. 10A). Similar increased levels were detected in the Δ*mrx6* Δ*pim1 Pestr-PIM1* double mutant, even at the start of the experiment, when Pim1 was still present. Strikingly, over the time course mtDNA levels did not further increase in cells lacking both proteins. This strongly supports a model in which Mrx6 acts via Pim1 to maintain WT mtDNA copy numbers.

Discussion

We identified new cellular components that modulate mtDNA levels in yeast using a forward genetic screen. We examined mtDNA levels in the 5148 mutants of a yeast deletion library and found that ~2% of these mutants had elevated levels of mtDNA compared to WT. Remarkably, the vast majority of these mutants (~85%) displayed less than a 2.5-fold increase in mtDNA levels, suggesting that a single gene deletion is not sufficient to more drastically alter mtDNA levels. This finding suggests that mtDNA copy number is under stringent regulation, which may be explained by a multi-layered system that involves a combination of various components, including factors regulating mtDNA replication and/or stability. One such layer that affects mtDNA levels is cell size, as the majority of our hits with elevated mtDNA copy number displayed increased cell size. This finding supports the notion that mtDNA copy number scales proportionally to mitochondrial network length, which in turn scales with cell volume (Rafelski *et al.*, 2012; Osman *et al.*, 2015). Therefore, in contrast to the nuclear genome, mtDNA copy number appears not to be determined on a 'per cell' basis, but rather on a 'per cell volume' basis. It remains an exciting task for future studies to unravel the molecular basis underlying the coordination between mitochondrial volume, mtDNA copy number and cell size.

Of the nine mutants that displayed elevated mtDNA levels and unaltered cell size, we examined the role of Mrx6 in maintenance of mtDNA levels. Mrx6 has been previously identified in a complex with the mitochondrial ribosome and named "Mitochondria oRganization of gene eXpression 6" (Kehrein *et al.*, 2015). However, to date the function of Mrx6 has remained obscure. Based on the following observations, Mrx6 appears directly linked to mtDNA copy number regulation: 1) Δ*mrx6* cells do not display a growth defect on a non-fermentable carbon source, ruling out that mtDNA levels are elevated due to a compensatory

feedback loop that responds to a defective respiratory chain, 2) Δ*mrx6* cells respond to a change in carbon source and display elevated mtDNA levels compared to WT on both fermentable and non-fermentable carbon sources, excluding the possibility that Δ*mrx6* cells are defective in glucose repression (Ulery *et al.*, 1994); 3) Δ*mrx6* cells do not exhibit any changes in mitochondrial network length or morphology, which excludes that increased mtDNA levels are caused by compromised mitochondrial structure. Thus, elevated mtDNA levels in Δ*mrx6* cells are not simply secondary effects caused by mitochondrial or cellular dysfunction.

Interestingly, deletion of *MRX6* resulted in elongated nucleoids. One plausible explanation for this phenotype is that newly replicated copies of mtDNA in Δ*mrx6* cells remain at least partially associated with parental mtDNA, resulting in bigger and misshapen nucleoids. The oblong shape of nucleoids is reminiscent of the proposed nucleoid division defects in *HSP60* mutants (Kaufman *et al.*, 2003). In line with this notion, we observed clustering of mtDNA copies when mtDNA was visualized with the mt-LacO-LacI system by structured illumination microscopy, which allowed detection and analysis of the spatial distribution of individual mtDNA copies. Alternatively, deletion of *MRX6* could change packaging of nucleoids, resulting in less compact and elongated nucleoids, which could alter mtDNA levels, perhaps by providing more access to the origins of replication.

Mrx6 contains a PET20 domain of uncharacterized structure and function that is conserved in fungi including distant species, such as *S. pombe*. Two other proteins in *S. cerevisiae*, Pet20 and Sue1, also belong to the PET20 protein family and localize to mitochondria (Wei and Sherman, 2004; Polevoda *et al.*, 2006). We see no alterations in mtDNA levels upon deletion of *PET20* or *SUE1*, alone or in combination, suggesting that both genes are

401 either required in other molecular contexts or only affect mtDNA copy number regulation to
402 minor extents.
403 Our protein interaction studies revealed a complex network comprised of the PET20
404 domain-containing proteins and the proteins Mam33 and Pim1. Mam33 was identified as an
405 Mrx6 interaction partner and is a specific translational activator of Cox1 mRNA (Roloff and
406 Henry, 2015). The physiological role of the interaction between Mrx6 and Mam33 is currently
407 unknown. However, the interaction points to a regulatory coordination between translation and
408 mtDNA copy number, which remains to be clarified in future studies. Interestingly, such a
409 coordination has been recently proposed for SLIMP, a specialized mitochondrial aminoacyl t-
410 RNA synthetase paralog, which affects mtDNA levels and interacts with the Pim1 Lon homolog
411 in arthropods (Picchioni *et al.*, 2019).
412 Remarkably, Mrx6, Pet20 and Sue1 are found in protein complexes that contain the
413 conserved mitochondrial Lon protease Pim1, which reveals a strong link between the PET20
414 domain-containing proteins and the mitochondrial protein quality control system. The finding
415 that co-purification of Pim1 with Pet20 depends on Mrx6 and that Mrx6 co-purifies with Pet20,
416 suggests that Pim1, Mrx6 and Pet20 may be part of the same complex. In contrast, Sue1 forms
417 an alternate complex with Pim1.
418 We consider it an attractive possibility that PET20 domain-containing proteins serve as
419 substrate specificity factors for Pim1. In agreement, Sue1 is required for degradation of labile
420 forms of cytochrome c (Wei and Sherman, 2004), suggesting that Sue1-Pim1 dependent
421 proteolysis could play a role in degradation of altered forms of cytochrome c (albeit it remains a
422 paradox how misfolded cytochrome c would venture into the mitochondrial matrix space to
423 meet its fate). By analogy, Mrx6 may be important for Pim1-dependent degradation of proteins

424 regulating mtDNA copy number. In support of this idea, we found that acute depletion of Pim1
425 results in elevated mtDNA levels matching those observed in Δ*mrx6* cells. However, depletion
426 of Pim1 in Δ*mrx6* cells did not lead to a further increase in mtDNA copy number, thus revealing
427 an epistatic relationship between Mrx6 and Pim1. These observations strongly support our
428 hypothesis that Mrx6 acts through Pim1 to regulate mtDNA levels.
429 Although we consider it an attractive hypothesis, we currently have no direct evidence
430 that mtDNA copy number is affected through the proteolytic activity of Pim1. However in
431 support of this notion, Pim1 has been shown to degrade multiple proteins involved in mtDNA
432 metabolism (Bayot *et al.*, 2010). For example, Abf2, a mtDNA packaging protein required for
433 mtDNA stablility, has been reported to be a substrate of Pim1 and changes in Abf2 protein
434 levels alter mtDNA copy number (Zelenaya-Troitskaya *et al.*, 1998; Bayot *et al.*, 2010).
435 Moreover, the ortholog of Abf2 in higher eukaryotes, TFAM, modulates mtDNA levels
436 (Ekstrand *et al.*, 2004; Kanki *et al.*, 2004), and changes in Lon protease expression alter mtDNA
437 copy number through degradation of TFAM (Matsushima *et al.*, 2010; Lu *et al.*, 2013). In our
438 hands, however, in Δ*mrx6* cells overall Abf2 protein levels did not change with respect to WT
439 cells, suggesting that the increased mtDNA phenotype in Δ*mrx6* cells would rely on subtle local
440 changes if Abf2 is a Mrx6-dependent Pim1 substrate (Supp. Fig. 10). Similarly, the human
441 mitochondrial protease Lon degrades the DNA helicase Twinkle (Kunova *et al.*, 2017).
442 Therefore, mtDNA copy number regulation by Mrx6-Pim1-dependent proteolysis might not be
443 limited to a single substrate.
444 Pim1 colocalizes with nucleoids (Kunova *et al.*, 2017), and its human homolog binds to
445 mtDNA, preferentially in the control region where mtDNA transcription and replication are
446 initiated (Lu *et al.*, 2007). While our localization studies support a Mrx6-dependent link

between Pim1 and mtDNA, our attempts to footprint the Pim1-Mrx6 complex on mtDNA by chromatin immunoprecipitation have been unsuccessful. Interestingly, we found Mrx6 complexes containing Pim1 and/or Pet20 in close vicinity of mtDNA, whereas the fraction of Mrx6 not colocalizing Pim1 and/or Pet20 was found predominately in DNA-free areas.

In summary, we propose the model in Figure 11: Mrx6 in complex with Pim1, Pet20 and Mam33 localizes to mtDNA. Mrx6 then facilitates substrate recognition of Pim1 and degradation of factors that stimulate mtDNA replication. Accordingly, absence of Mrx6 would lead to an accumulation of such factors and in turn increase the number of mtDNA in the organelle.

Mitochondria evolved as endosymbionts from ancestral bacteria. In this light, it is exciting that Lon proteases are also involved in regulating replication of bacterial genomes. *C. crescentus* and *E.coli* Lon proteases, for example, affect DNA replication by degrading a replication initiation factor and an inhibitor, respectively (Langklotz and Narberhaus, 2011; Jonas *et al.*, 2013). Therefore, our results identify a novel component in an evolutionarily conserved regulatory mechanism of mtDNA replication.

Material and Methods

Yeast strains and plasmids

Yeast strains used in this study are derived from W303 and are listed in Table S2. Deletion of yeast genes was performed in diploid strains and C-terminal tagging of genes was done in haploid strains using homologous recombination as described previously (Janke *et al.*, 2004). Haploid cells were used for all experiments, except those shown in Figs. 2A, 3 and 4 where diploids cells were used. Plasmids and oligonucleotides used in this study are listed in Table S3 and Table S4, respectively.

Colony blot hybridization

A previously described protocol (Kleinman, 1996) was followed with minor additions to optimize the protocol for fluorescent hybridization. Briefly, the mutants of the yeast deletion library were grown on glucose rich agar plates and transferred to nylon membranes (Bright Star-plus was used for the 1st and 2nd screens and Pall Biodyne A was used for the 3rd screen) by incubating membranes on plates for 5 min followed by gentle lifting. Membranes were air dried for 5 min and placed, colony side up, on Whatman 3M papers that were soaked with reducing buffer (1M Sorbitol, 50 mM DTT, 20 mM EDTA, 10 mM NaAzide, 10 mM KF) and kept at RT for 20 min. Subsequently, membranes were transferred onto Whatman 3M papers that were soaked with lysis buffer (1 M Sorbitol, 10 mM DTT, 20 mM EDTA, 10 mM Tris-HCl pH=7.6, 10 mM NaAzide, 10 mM KF, 3mg/ml zymolyase 20-T) and kept at 37 °C in a closed container overnight. The next day, membranes were placed on Whatman 3M papers that were soaked with 0.5 M NaOH for 10 min. Membranes were air dried for 5 min and neutralized by incubating on Whatman 3M papers saturated with 0.5 M Tris-HCl pH=7.5/ 5X SSC for 5 min, 2 times, and

484 transferred onto Whatman 3MM papers saturated with TE pH=7.5 / 1X SSC (150mM NaCl,
485 15mM sodium citrate) for 5 min. Following neutralization, membranes were placed on
486 Whatman 3MM papers soaked with TE pH=7.5 / 1X SSC buffer with 0.2 mg/ml RNaseA
487 (Sigma) and kept in a closed container for 2 hours at 37 °C. Subsequently, membranes were
488 placed on Whatman 3MM papers that were soaked with 100 mM Tris-HCl pH=7.5 / 1X SSC
489 for 5 min for 2 times, air dried and baked at 65 °C for 30 min, followed by UV-crosslinking at
490 60 mJ/cm^2 with 254 nm irradiation. Membranes were placed into hybridization bottles and
491 washed 2 times with 5X SSC, 0.5% SDS, 10 mM EDTA for 15 min while rotating at 65 °C.
492 Membranes were rinsed with Proteinase K buffer (50mM Tris HCl pH=7.5, 10 mM EDTA, 1%
493 SDS, 50 mM NaCl) and incubated in Proteinase K buffer containing 2 mg/ml Proteinase K
494 (Invitrogen) for 2 h at 55 °C. Membranes were rinsed with 5X SSC and washed with 3M Urea,
495 1% SDS at 55 °C, 3 times for 10 min each. Membranes were further washed with 5X SSC 2
496 times for 15 min each and pre-hybridized for 2 hours with hybridization buffer (50%
497 Formamide, 8% Dextran Sulfate, 2.5X SSC, 5 mM EDTA, 25 mM Hepes-KOH pH=7, 3%
498 SDS) at 42 °C. Membranes were hybridized with fluorescently labeled probes (final
499 concentration 100ng/ml of mtDNA-Cy3 probe mix and 100ng/ml nuclear DNA-Cy5 probe mix)
500 in hybridization buffer at 42 °C overnight. The next day, membranes were washed with wash
501 buffer (1X SSC, 1% SDS) 3 times for 10 min each at 65 °C. Membranes were completely air
502 dried prior to scanning with a Typhoon Fluorescent Scanner using Cy3 and Cy5 channels in
503 normal sensitivity.

504 **Preparation of probes for hybridization**

505 Probes were prepared by PCR using Phusion DNA Polymerase and different pairs of
506 primers (Table S4). 12 different probes were pooled to detect nuclear DNA and 2 different

probes were pooled to detect mtDNA. PCR products were cleaned-up and concentrated with Zymo DNA Clean & Concentrator-5 and labeled with Mirus *Label* IT Nucleic Acid Labeling Kits using Cy3 or Cy5 dyes overnight according to the product manual. Labeled probes were EtOH precipitated and stored at -30 °C. Probes were boiled for 5 mins before addition into hybridization buffer.

Quantification of colony blots

Scans of colony blots were quantified with ImageJ. The median signal intensity of each colony, for Cy3 and Cy5 channels, was determined after background subtraction by using a rolling ball plugin. Auto-fluorescence of yeast colonies was measured in both channels from a sample membrane that had not been incubated with probes. Auto-fluorescence of colonies linearly correlated with colony size, and thus we developed an algorithm that calculates auto-fluorescence for each mutant depending on its colony size. The hybridization signal for each colony was calculated by subtracting the estimated auto-fluorescence from the median signal intensity. However, later we found out that auto-fluorescence also correlates with respiratory capability, which explains why the mutants that lack mtDNA have mtDNA/nDNA ratios below zero after subtraction of colony auto-fluorescence. To calculate relative fold changes in mtDNA/nDNA ratios, mtDNA/nDNA ratios of all mutants except the ones that had lost mtDNA were averaged and used for normalization of each mutant mtDNA/nDNA ratio.

Cell growth and quantitative PCR

Prior to harvesting, yeast cells were grown in liquid media (YPD, YPEG or drop-out synthetic media) in log-phase for 24 hours at 30 °C. In Fig. 2C, cells were treated with 0.5mM H_2O_2 in YPD for 1 hour. In Fig. 2D, cells were treated with DMSO or FCCP (5ug/ml) in YPD

for 1 hour. Genomic DNA (gDNA) was extracted using the Thermo Scientific Pierce Yeast DNA Extraction Reagent or Zymo ZR-96 Fungal/Bacterial DNA kits. gDNA was subjected to qPCR using iQ- Syber Green Supermix (Bio-RAD) and primers specific for Cox1 and Act1 genes according to the manufacturer's manual (Table S4). For absolute mtDNA copy number quantification, 1kb fragments of Cox1 and Act1 genes were cloned into pUC19 plasmids and used as standards for copy number quantification. For statistical analysis of qPCR data, unpaired t test was used for comparison of two groups and one-way ANOVA was used for multiple comparisons, followed by Tukey's multiple comparison test in GraphPad Prism.

Flow cytometry

Yeast cells were grown in liquid media (YPD) in 96-well polystyrene plates overnight at 30° C, and the next morning diluted, regrown for ~4 doubling times and harvested at OD_{600}=~0.5-1. Yeast cultures were then transferred to 96-well microplates (Corning), diluted with YPD one to five ratio and analyzed by a flow cytometer (LSR II, Beckton-Dickinson), and a high throughput sampler (BD High Throughput Sampler, Beckton-Dickinson) to inject samples into the flow cytometer. The SSC-H parameter was used as an estimate of cell size and the SSC-H values of the mutants were normalized to the value of WT. Cell size of some mutants was also analyzed by microscopy to verify cell size increase. The remaining cultures were used for gDNA isolation and subjected to qPCR for mtDNA analysis for Fig. 1D.

Growth analysis

Yeast cells were grown in liquid media (YPD) in log-phase for 24 hours at 30 °C and diluted to OD_{600} =0.05 in total 100 µl YPD or diluted to OD_{600} =0.1 in total 100 µl YPEG in a 96-well clear bottom microplate (Corning). The wells on the edges of the plate were filled with

YPD to maintain humidity and the lid was secured by using a tape that partially covered the plate to allow air exchange. Growth assays were conducted at 30 °C by using Tecan Infinite 200 Pro plate reader for 48 hours with a kinetic interval of 15 min.

Immunoprecipitation

Immunoprecipitations were performed as previously described (Friedman *et al.*, 2015). Briefly, 500 OD_{600} cells grown in log-phase in YPD at 30 °C, were harvested by centrifugation, resuspended in 5 ml of lysis buffer (20 mM HEPES pH=7.4, 150 mM KOAc, 2 mM $Mg(OAc)_2$, 1 mM EGTA, 0.6 M sorbitol), and protease inhibitor cocktail was added to 1x (EDTA free, Roche). Cell suspension was flash-frozen dropwise in liquid N_2, and lysed using a ball mill (Retsch MM301). The cell powder was thawed in RT, and unbroken cells and large debris were pelleted using GH-3.8 rotor at 1500 rpm for 5 min at 4 °C. For solubilization, digitonin was added to the supernatant to a final concentration of 1%. Samples were incubated for 30 min at 4 °C, and cleared by centrifugation at 12,000 x g at 4 °C. 50 µl µMACS anti-Flag beads (Miltenyi Biotec) were added to the supernatant and incubated 45 min at 4 °C, followed by isolation with µ columns and a µMACS separator (Miltenyi Biotec). Columns were washed 3 times with lysis buffer, 0.1% digitonin and 1x protease inhibitor, and 2 times with only lysis buffer. Samples were eluted using on-bead trypsin digest by incubating beads with 25 µl of elution buffer I (2M Urea, 50 mM Tris-HCl pH=7.5, 1mM DTT and 5 µg/ml trypsin (Trypsin Gold, Promega)) for 30 min at RT. 50 µl of elution buffer II (2M Urea, 50 mM Tris-HCl, pH=7.5, 5 mM chloroacetamide) was added to the column, 2 times, to collect elutions. Elutions were kept at RT overnight to continue digestion. Mass spectrometric proteomic analysis was performed at the Genome Center Proteomics Core of the University of California, Davis.

Western Blot analysis

For Fig. 7A, the samples eluted from the μMACS beads by incubating beads with preheated (95 °C) 1x SDS loading buffer instead of trypsin digestion. For Figs. 2A and Supp. 8, proteins were extracted from 1 OD_{600} cells in Urea-CHAPS buffer (20mM Tris-HCl pH=7.4, 7 M Urea, 2 M thiourea, 4% CHAPS) by 3 min bead beating at 4 °C. Protein concentration of each sample was measured by Pierce BCA protein assay kit (Thermo Scientific). Samples were boiled for 5 min in SDS loading dye and BME prior to SDS-PAGE analysis, transferred to nitrocellulose membrane, and immuno-blotted with the following primary antibodies at the indicated concentrations in 5% milk PBS-T/TBS-T buffer: mouse anti-FLAG M2 (1:5000, Sigma–Aldrich); rabbit anti-Pim1 (1:1000, kindly provided by C. Suzuki); mouse anti-myc 9E10 (1:1000, Santa Cruz); mouse anti-PGK1 (1:5000, abcam); rabbit anti-Tom40 (1:30000, kindly provided by T. Langer); rabbit anti-Abf2 (1:1000, kindly provided by J. Nunnari); rabbit anti Tim50 (Mokranjac *et al.*, 2003) (1:1000, kindly provided by K. Hell).

SI microscopy and analysis

For Fig. 3A, slides were prepared as previously described (Kaplan and Ewers, 2015). Briefly, microscope coverslips (High Precision) were cleaned with a plasma cleaner (PDC-001, Harrick Plasma) and treated with concanavalin A (Sigma; 5mg/ml) for 30 min, spin-coated for 15 sec and air-dried for 15 min in a vacuum desiccator. Prior to imaging, yeast cells were grown in liquid drop-out synthetic media in log-phase for 24 hours at 30 °C. 0.5 OD_{600} cells were spun down, washed and resuspended in 100 μl PBS. 20 μl cell suspension was added on the concanavalin A treated coverslips and incubated for 15 min. Unattached cells were washed with PBS. For fixation, cells were incubated twice for 5 min with 4% paraformaldehyde (Electron

595 Microscopy Sciences) in PBS on coverslips. Fixation was followed by quenching with 50 mM
596 NH_4Cl, 2 times, 10 min each. Cells were washed with PBS and a drop of anti-fade media
597 (Vectashield) was added before mounting coverslips to slides. Slides were imaged using
598 DeltaVision OMX SR (GE) using SIM mode and a 60x/1.42 NA oil objective. The Imaris
599 software was used to detect/count LacI-GFP foci and to segment the mitochondrial network in
600 three dimensions. Quantification of mitochondrial network length, mitochondrial endpoints and
601 distribution of mtDNA was performed as described previously (Osman *et al.*, 2015). Three- or
602 four-way junctions of the segmented mitochondrial network were scored as branchpoints.
603 For Fig. 4A, yeast cells were grown in liquid drop-out synthetic media in log-phase for
604 24 h at 30 °C and fixed with 4% paraformaldehyde (Electron Microscopy Sciences) in growth
605 media for 30 min at RT. Cells were prepared as described previously (Silver, 2009). Briefly,
606 cells were pelleted and washed 2 times with P solution (0.1M $KHPO_4$, 1.2M Sorbitol) and
607 resuspended in 1 ml of P solution. 15 µl of 10 mg/ml zymolyase (T-20) and 5 µl BME were
608 added to the solution, and incubated at RT for 30 min. Cells were gently washed with P solution
609 once and resuspended in 0.5 ml of P solution. Microscope coverslips (High Precision) were
610 plasma cleaned and coated with 0.1% poly-L-lysine for 20 min. Coverslips were washed 2 times
611 with ddH_2O and air dried completely. 30 µl of cell suspension was added and incubated 20 min.
612 Excess media were aspirated and coverslips were plunged into ice-cold methanol for 6 mins,
613 followed by submerging into ice-cold acetone for 30 sec. Coverslips were air dried briefly and
614 incubated with 3% BSA (Sigma) in PBS for 1 h at RT. Cells were stained with DAPI
615 (Invitrogen; 5 µg/ml) for 5 min and washed 2 times with PBS. Coverslips were mounted to
616 slides after addition of a drop of anti-fade medium (Vectashield). Slides were imaged using
617 DeltaVision OMX SR (GE) using SIM mode and a 60x/1.42 NA oil objective. The Imaris

618 software was used to calculate the number of DAPI stained-nucleoids and the volume of each
619 nucleoid in three dimensions.

620 **Immunofluorescence and analysis**

621 Cells were prepared for immunofluorescence as it was done before for the cells shown in
622 Fig. 4A, except after acetone treatment cells were incubated with blocking buffer, 3% Goat
623 Serum (Jackson ImmunoResearch) in PBS for 1 h at RT, followed by incubation with mouse
624 anti-DNA antibody (1:1000, abcam) in blocking buffer overnight at 4 °C. The next day, cells
625 were washed 3 times with blocking buffer and incubated with anti-mouse secondary antibody
626 conjugated with Alexa Fluor 405 (1:500) or Alexa Fluor 647 (1:1000) for an hour and a half at
627 RT at dark. Subsequently, cells were washed 3 times with blocking buffer and 2 times with
628 PBS, and if necessary stained with DAPI (5µg/ml) for 5 min and washed 2 times with PBS.
629 Coverslips were mounted to slides after addition of a drop of anti-fade medium (Vectashield).
630 Slides were imaged using DeltaVision OMX SR (GE) using conventional mode and a 60x/1.42
631 NA oil objective. Deconvolution of images and maximum projection of Z stacks done by using
632 DeltaVision SoftWorRx. Quantification of nucleoid length was performed as follows. First, a
633 curved line was manually drawn through the mitochondrial network of each cell and the line's
634 one-dimensional intensity profile was extracted. Then, nucleoids were automatically picked out
635 from the intensity profile by adaptive thresholding. Local threshold values were individually
636 calculated for each data point using Li's minimum cross entropy method applied within a 4.8
637 µm long sliding window (Li, 1993). The sliding window approach allowed us to compensate for
638 nonuniform fluorescent background in the images and to robustly identify peaks in the intensity
639 profile in an unbiased way (Supp. Fig. 3A). We carried out our experiments to determine the
640 length of nucleoids using both conventional and super-resolution (structured illumination)

641 microscopy (Fig. 4) and found that the increase in nucleoid length in Δ*mrx6* cells is robustly
642 detected by both methods.

643 **Live microscopy and analysis**

644 Microscope coverslips (High Precision) were plasma cleaned and treated with
645 concanavalin A (0.5 mg/ml) for 15 min, spin-coated for 15 sec and air-dried for 15 min in a
646 vacuum desiccator. Prior to imaging, yeast cells were grown in liquid drop-out synthetic media
647 in log-phase for 24 h. DAPI was added to media (1 µg/ml final concentration) for 15 min if
648 needed. 0.5 OD_{600} cells were spun down, washed and resuspended in 20 µl drop-out synthetic
649 media lacking sugar. Cell suspension was added on the concanavalin A-treated cover slips and
650 incubated for 5 min. Unattached cells were washed with drop-out synthetic media. Slides were
651 imaged using DeltaVision OMX SR (GE) using conventional mode and a 60x/1.42 NA oil
652 objective. Deconvolution of images and maximum projection of Z stacks done by using
653 DeltaVision SoftWorRx. Intensity profiles were obtained with ImageJ by measuring pixel
654 intensities along mitochondrial tubules of Z-projected images using the line draw tool (settings:
655 line width=3). Intensity profiles along identical lines from different channels were used to
656 calculate the Pearson's Correlation Coefficients (PCC) (Supp. Fig. 5C). The Manders'
657 Colocalization Coefficients (MCC) were calculated after thresholding intensity profiles using
658 Yen's method (Yen *et al.*, 1995). To assess significance of colocalizations, MCC and PCC were
659 determined for intensity profiles of two channels, of which one intensity profile was randomized
660 by scrambling blocks of 5 values (400 nm) in the line profiles. Scrambling blocks of values
661 rather than single values has been shown to give a more accurate probability distribution,
662 because it retains autocorrelation between neighboring pixels (Costes *et al.*, 2004). Statistical

significance of PCC and MCC values between measured and randomized intensity profiles was determined by applying the independent t-test.

To test whether fractions of Mrx6 or Pet20 that colocalize with Pim1 preferentially colocalize with DAPI, intensity profiles for Mrx6-Neon or Pet20-Neon and Pim1-Ruby were first thresholded with Yen's method and then multiplied with one another. Values greater than 0 in the resulting profile were scored as colocalizing fractions, whereas values equal to 0 were scored as non-colocalizing fractions. MCC values between colocalizing or non-colocalizing fractions of Mrx6-Neon-Pim1-Ruby or Pet20-Neon-Pim1-Ruby and DAPI were determined as described in the previous paragraph. To assess significance of this analysis, the same analysis was performed with a randomized DAPI profile. A t-test was used to infer statistical significance between MCC values determined for the real data and the randomized data.

Acute depletion of Pim1

For expression of proteins under the control of an estradiol regulatable expression system we assembled pCO450 in multi-step NEBuilder (New England Biolabs) cloning procedures. The previous reported plasmid encoded components of an established yeast estradiol expression system 'P*ACT1*(-1-520)-LexA-ER-haB42-T*CYC1*' (FPR718) and 'insul-(*lexA*-box)2-Pmin*CYC1*-CitrineA206K-T*CYC1*' (FPR792) (Ottoz *et al.*, 2014) were combined on one plasmid followed by a SphI/NheI cloning site for integration of the target gene in combination with a KanMX6 selection marker. The construct was flanked with two homology regions that enable stable genomic integration into the yeast HO locus to omit irregular expressions within the culture owing to alterations in plasmid quantity in different cells. From this plasmid (pCO450) estradiol regulatable Pim1-strains were generated by construction of pCO460. The open reading frame of *PIM1* was amplified from genomic DNA using forward

686 primer 5'-CTATACTAGTGGATCCGCATGCTAAGAACAAGAACCACAAAGA-3' and
687 reverse primer 5'-
688 CATAACTAATTACATGAGCTAGCGTTAGTCCTTTTCCTTTTTAGCATCCAA-3' and
689 introduced into the SphI-linearized pCO450 backbone by NEBuilder reaction. The resulting
690 plasmid was linearized by NotI digestion and genomically integrated into the HO locus of WT
691 cells (yCO363) by transformation and subsequent G418 selection (yCO575). The endogenous
692 *PIM1* locus was deleted afterwards via homologous recombination and a hygromycin marker as
693 described previously (Janke *et al.*, 2004), resulting in yCO593. Strains were continuously
694 maintained on medium containing β-Estradiol (Alfa Aesar). By maintaining Pim1 expression
695 we could circumvent pleiotropic effects that manifest once the endogenous copy of *PIM1* is
696 deleted. The double mutant yCO600 was generated by additionally deleting *MRX6* with a
697 nourseothricin selection marker.
698 For experiments presented in Fig. 10 cells were grown in liquid culture at log-phase in
699 synthetic complete medium (SC) containing 2 % glucose supplemented with 25 nM β-Estradiol.
700 To acutely deplete Pim1 expression, cells were washed and estradiol omitted from the medium.
701 Cultures were permanently maintained in log-phase and harvested at an OD_{600}=1 at each time
702 point. For DNA and protein extraction 2.5 OD_{600} cells were harvested, washed with Milli-Q
703 water and frozen immediately. Total DNA was extracted as previously reported by bead
704 breaking in the presence of phenol/chloroform/isoamyl alcohol (Hoffman, 1997). mtDNA copy
705 number was determined by quantitative PCR using iQ- Syber Green Supermix (Bio-RAD) as
706 described in the previous paragraph "Cell growth and quantitative PCR".

707 **Online supplemental material**

Figs. S1-10 are supplementary to main figures and Tables S1-4 showing the list of the mutants identified in each screen, yeast strains and plasmids created or used, and oligonucleotides used in this study. The Python scripts, used for colocalization analyses (Figs. 6, 8 and 9), and measuring length of nucleoids (Supp. Fig. 3) are also included in the online supplemental materials.

Acknowledgments

We thank Jodi Nunnari, David Morgan, Wallace Marshall, Patrick O'Farrell and members of the Walter lab for their technical advice and insightful discussions. We thank Carolyn Suzuki for providing the anti-Pim1 antibody, Jodi Nunnari for the anti-Abf2 antibody, Thomas Langer for the anti-Tom40 antibody and Kai Hell for the anti-Tim50 antibody, Fabian Rudolf for plasmids FRP718 and FRP792, Voytek Okreglak, Hansong Ma, Jeiwei Xu, Jason Wojcechowskyj, Ingacio Zuleta, Ricardo Almeida, Amy Chang, Shoshana Brown, Samantha Lewis, Justin M. Yamada for reagents, technical advice and their helpful discussions, Anne Pipathsouk and Roberto Diaz for their technical help during their rotation and internship, respectively. We thank Tanja Kautzleben for her technical assistance. We also thank Nikon Imaging Center at UCSF and Proteomics Core Facility at UC Davis for their invaluable contributions. This work was supported by a UCSF Zaffaroni Fellowship (to AG) and Howard Hughes Medical Institute (HHMI) International Student Research Fellowships (to AG and AM). VB is a Damon Runyon Fellow supported by the Damon Runyon Cancer Research Foundation (DRG-2284-17). CO was funded by the Simons Foundation (# 326844). CO and SS are supported by a grant from the European Research Council (ERCStG-714739 IlluMitoDNA). PW is a HHMI Investigator. The authors declare no competing financial interests.

Author contributions

Aylin Göke: Conceptualization, Data curation, Formal analysis, Validation, Investigation, Visualization, Methodology, Writing—original draft, Writing—review and editing; Simon Schrott: Conceptualization, Formal analysis, Validation, Investigation, Visualization, Methodology, Writing—review and editing; Arda Mizrak: Conceptualization, Formal analysis, Software; Vladislav Belyy: Conceptualization, Formal analysis, Software, Supervision, Writing—review and editing; Christof Osman: Conceptualization, Resources, Data curation, Formal analysis, Validation, Investigation, Visualization, Methodology, Software, Supervision, Writing—original draft, Writing—review and editing; Peter Walter: Conceptualization, Funding acquisition, Resources, Supervision, Writing—review and editing

References

Bayot, A., Gareil, M., Rogowska-Wrzesinska, A., Roepstorff, P., Friguet, B., and Bulteau, A.L. (2010). Identification of novel oxidized protein substrates and physiological partners of the mitochondrial ATP-dependent Lon-like protease Pim1. The Journal of biological chemistry *285*, 11445-11457.

Brown, T.A., Tkachuk, A.N., Shtengel, G., Kopek, B.G., Bogenhagen, D.F., Hess, H.F., and Clayton, D.A. (2011). Superresolution fluorescence imaging of mitochondrial nucleoids reveals their spatial range, limits, and membrane interaction. Mol Cell Biol *31*, 4994-5010.

Chen, X.J., and Butow, R.A. (2005). The organization and inheritance of the mitochondrial genome. Nat Rev Genet *6*, 815-825.

Clay Montier, L.L., Deng, J.J., and Bai, Y. (2009). Number matters: control of mammalian mitochondrial DNA copy number. J Genet Genomics *36*, 125-131.

Connelly, C.F., and Akey, J.M. (2012). On the prospects of whole-genome association mapping in Saccharomyces cerevisiae. Genetics *191*, 1345-1353.

Conrad, M.N., and Newlon, C.S. (1982). The regulation of mitochondrial DNA levels in Saccharomyces cerevisiae. Curr Genet *6*, 147-152.

Costes, S.V., Daelemans, D., Cho, E.H., Dobbin, Z., Pavlakis, G., and Lockett, S. (2004). Automatic and quantitative measurement of protein-protein colocalization in live cells. Biophys J *86*, 3993-4003.

Ekstrand, M.I., Falkenberg, M., Rantanen, A., Park, C.B., Gaspari, M., Hultenby, K., Rustin, P., Gustafsson, C.M., and Larsson, N.G. (2004). Mitochondrial transcription factor A regulates mtDNA copy number in mammals. Hum Mol Genet *13*, 935-944.

Friedman, J.R., Mourier, A., Yamada, J., McCaffery, J.M., and Nunnari, J. (2015). MICOS coordinates with respiratory complexes and lipids to establish mitochondrial inner membrane architecture. Elife *4*.

Fukuoh, A., Cannino, G., Gerards, M., Buckley, S., Kazancioglu, S., Scialo, F., Lihavainen, E., Ribeiro, A., Dufour, E., and Jacobs, H.T. (2014). Screen for mitochondrial DNA copy number maintenance genes reveals essential role for ATP synthase. Mol Syst Biol *10*, 734.

Giaever, G., Chu, A.M., Ni, L., Connelly, C., Riles, L., Véronneau, S., Dow, S., Lucau-Danila, A., Anderson, K., André, B., Arkin, A.P., Astromoff, A., El Bakkoury, M., Bangham, R., Benito, R., Brachat, S., Campanaro, S., Curtiss, M., Davis, K., Deutschbauer, A., Entian, K.-D., Flaherty, P., Foury, F., Garfinkel, D.J., Gerstein, M., Gotte, D., Güldener, U., Hegemann, J.H., Hempel, S., Herman, Z., Jaramillo, D.F., Kelly, D.E., Kelly, S.L., Kötter, P., LaBonte, D., Lamb, D.C., Lan, N., Liang, H., Liao, H., Liu, L., Luo, C., Lussier, M., Mao, R., Menard, P., Ooi, S.L., Revuelta, J.L., Roberts, C.J., Rose, M., Ross-Macdonald, P., Scherens, B., Schimmack, G., Shafer, B., Shoemaker, D.D., Sookhai-Mahadeo, S., Storms, R.K., Strathern, J.N., Valle, G., Voet, M., Volckaert, G., Wang, C.-y., Ward, T.R., Wilhelmy, J., Winzeler, E.A., Yang, Y., Yen, G., Youngman, E., Yu, K., Bussey, H., Boeke, J.D., Snyder, M., Philippsen, P., Davis, R.W., and Johnston, M. (2002). Functional profiling of the Saccharomyces cerevisiae genome. Nature *418*, 387-391.

Hoffman, C.S. (1997). Preparation of Yeast DNA *39*, 13.11.11-13.11.14.

Ikeda, M., Ide, T., Fujino, T., Arai, S., Saku, K., Kakino, T., Tyynismaa, H., Yamasaki, T., Yamada, K., Kang, D., Suomalainen, A., and Sunagawa, K. (2015). Overexpression of TFAM or twinkle increases mtDNA copy number and facilitates cardioprotection associated with limited mitochondrial oxidative stress. PLoS One *10*, e0119687.

Jajoo, R., Jung, Y., Huh, D., Viana, M.P., Rafelski, S.M., Springer, M., and Paulsson, J. (2016). Accurate concentration control of mitochondria and nucleoids. Science *351*, 169-172.
Janke, C., Magiera, M.M., Rathfelder, N., Taxis, C., Reber, S., Maekawa, H., Moreno-Borchart, A., Doenges, G., Schwob, E., Schiebel, E., and Knop, M. (2004). A versatile toolbox for PCR-based tagging of yeast genes: new fluorescent proteins, more markers and promoter substitution cassettes. Yeast *21*, 947-962.
Jonas, K., Liu, J., Chien, P., and Laub, M.T. (2013). Proteotoxic stress induces a cell-cycle arrest by stimulating Lon to degrade the replication initiator DnaA. Cell *154*, 623-636.
Kanki, T., Ohgaki, K., Gaspari, M., Gustafsson, C.M., Fukuoh, A., Sasaki, N., Hamasaki, N., and Kang, D. (2004). Architectural role of mitochondrial transcription factor A in maintenance of human mitochondrial DNA. Mol Cell Biol *24*, 9823-9834.
Kaplan, C., and Ewers, H. (2015). Optimized sample preparation for single-molecule localization-based superresolution microscopy in yeast. Nat Protoc *10*, 1007-1021.
Kaufman, B.A., Kolesar, J.E., Perlman, P.S., and Butow, R.A. (2003). A function for the mitochondrial chaperonin Hsp60 in the structure and transmission of mitochondrial DNA nucleoids in Saccharomyces cerevisiae. J Cell Biol *163*, 457-461.
Kehrein, K., Schilling, R., Moller-Hergt, B.V., Wurm, C.A., Jakobs, S., Lamkemeyer, T., Langer, T., and Ott, M. (2015). Organization of Mitochondrial Gene Expression in Two Distinct Ribosome-Containing Assemblies. Cell Rep 10(6):843-853.
Kleinman, M.J. (1996). Yeast colony hybridization. Methods Mol Biol *53*, 189-192.
Kornblum, C., Nicholls, T.J., Haack, T.B., Schöler, S., Peeva, V., Danhauser, K., Hallmann, K., Zsurka, G., Rorbach, J., Iuso, A., Wieland, T., Sciacco, M., Ronchi, D., Comi, G.P., Moggio, M., Quinzii, C.M., DiMauro, S., Calvo, S.E., Mootha, V.K., Klopstock, T., Strom, T.M., Meitinger, T., Minczuk, M., Kunz, W.S., and Prokisch, H. (2013). Loss-of-function mutations in MGME1 impair mtDNA replication and cause multisystemic mitochondrial disease. Nature Genetics *45*, 214.
Kukat, C., Wurm, C.A., Spåhr, H., Falkenberg, M., Larsson, N.-G., and Jakobs, S. (2011). Super-resolution microscopy reveals that mammalian mitochondrial nucleoids have a uniform size and frequently contain a single copy of mtDNA *108*, 13534-13539.
Kunova, N., Ondrovicova, G., Bauer, J.A., Bellova, J., Ambro, L., Martinakova, L., Kotrasova, V., Kutejova, E., and Pevala, V. (2017). The role of Lon-mediated proteolysis in the dynamics of mitochondrial nucleic acid-protein complexes. Sci Rep *7*, 631.
Langklotz, S., and Narberhaus, F. (2011). The Escherichia coli replication inhibitor CspD is subject to growth-regulated degradation by the Lon protease. Mol Microbiol *80*, 1313-1325.
Lewis, S.C., Uchiyama, L.F., and Nunnari, J. (2016). ER-mitochondria contacts couple mtDNA synthesis with mitochondrial division in human cells. Science *353*, aaf5549.
Li, C.H., and C.K. Lee. (1993). Minimum Cross Entropy Thresholding. Pattern Recognition *26*, 617-625.
Lipinski, K.A., Kaniak-Golik, A., and Golik, P. (2010). Maintenance and expression of the S. cerevisiae mitochondrial genome--from genetics to evolution and systems biology. Biochim Biophys Acta *1797*, 1086-1098.
Liu, C.-S., Cheng, W.-L., Lee, C.-F., Ma, Y.-S., Lin, C.-Y., Huang, C.-C., and Wei, Y.-H. (2006). Alteration in the copy number of mitochondrial DNA in leukocytes of patients with mitochondrial encephalomyopathies. Acta Neurologica Scandinavica *113*, 334-341.

Lu, B., Lee, J., Nie, X., Li, M., Morozov, Y.I., Venkatesh, S., Bogenhagen, D.F., Temiakov, D., and Suzuki, C.K. (2013). Phosphorylation of human TFAM in mitochondria impairs DNA binding and promotes degradation by the AAA+ Lon protease. Mol Cell *49*, 121-132.
Lu, B., Yadav, S., Shah, P.G., Liu, T., Tian, B., Pukszta, S., Villaluna, N., Kutejova, E., Newlon, C.S., Santos, J.H., and Suzuki, C.K. (2007). Roles for the human ATP-dependent Lon protease in mitochondrial DNA maintenance. The Journal of biological chemistry *282*, 17363-17374.
MacAlpine, D.M., Perlman, P.S., and Butow, R.A. (2000). The numbers of individual mitochondrial DNA molecules and mitochondrial DNA nucleoids in yeast are co-regulated by the general amino acid control pathway. EMBO J *19*, 767-775.
Major, T., von Janowsky, B., Ruppert, T., Mogk, A., and Voos, W. (2006). Proteomic analysis of mitochondrial protein turnover: identification of novel substrate proteins of the matrix protease pim1. Mol Cell Biol *26*, 762-776.
Matsushima, Y., Goto, Y., and Kaguni, L.S. (2010). Mitochondrial Lon protease regulates mitochondrial DNA copy number and transcription by selective degradation of mitochondrial transcription factor A (TFAM). Proc Natl Acad Sci U S A *107*, 18410-18415.
Meeusen, S., and Nunnari, J. (2003). Evidence for a two membrane-spanning autonomous mitochondrial DNA replisome. J Cell Biol *163*, 503-510.
Mengel-From, J., Thinggaard, M., Dalgård, C., Kyvik, K.O., Christensen, K., and Christiansen, L. (2014). Mitochondrial DNA copy number in peripheral blood cells declines with age and is associated with general health among elderly. Human Genetics *133*, 1149-1159.
Miller, F.J., Rosenfeldt, F.L., Zhang, C., Linnane, A.W., and Nagley, P. (2003). Precise determination of mitochondrial DNA copy number in human skeletal and cardiac muscle by a PCR-based assay: lack of change of copy number with age. Nucleic acids research *31*, e61.
Mokranjac, D., Paschen, S.A., Kozany, C., Prokisch, H., Hoppins, S.C., Nargang, F.E., Neupert, W., and Hell, K. (2003). Tim50, a novel component of the TIM23 preprotein translocase of mitochondria. The EMBO Journal *22*, 816-825.
Osman, C., Noriega, T.R., Okreglak, V., Fung, J.C., and Walter, P. (2015). Integrity of the yeast mitochondrial genome, but not its distribution and inheritance, relies on mitochondrial fission and fusion. Proc Natl Acad Sci U S A *112*, E947-956.
Ottoz, D.S., Rudolf, F., and Stelling, J. (2014). Inducible, tightly regulated and growth condition-independent transcription factor in Saccharomyces cerevisiae. Nucleic acids research *42*, e130.
Picchioni, D., Antolin-Fontes, A., Camacho, N., Schmitz, C., Pons-Pons, A., Rodríguez-Escribà, M., Machallekidou, A., Güler, M.N., Siatra, P., Carretero-Junquera, M., Serrano, A., Hovde, S.L., Knobel, P.A., Novoa, E.M., Solà-Vilarrubias, M., Kaguni, L.S., Stracker, T.H., and Ribas de Pouplana, L. (2019). Mitochondrial Protein Synthesis and mtDNA Levels Coordinated through an Aminoacyl-tRNA Synthetase Subunit. Cell Reports *27*, 40-47.e45.
Polevoda, B., Panciera, Y., Brown, S.P., Wei, J., and Sherman, F. (2006). Phenotypes of yeast mutants lacking the mitochondrial protein Pet20p. Yeast *23*, 127-139.
Pyle, A., Anugrha, H., Kurzawa-Akanbi, M., Yarnall, A., Burn, D., and Hudson, G. (2016). Reduced mitochondrial DNA copy number is a biomarker of Parkinson's disease. Neurobiol Aging *38*, 216 e217-216 e210.

Rafelski, S.M., Viana, M.P., Zhang, Y., Chan, Y.H., Thorn, K.S., Yam, P., Fung, J.C., Li, H., Costa Lda, F., and Marshall, W.F. (2012). Mitochondrial network size scaling in budding yeast. Science *338*, 822-824.
Roloff, G.A., and Henry, M.F. (2015). Mam33 promotes cytochrome c oxidase subunit I translation in Saccharomyces cerevisiae mitochondria. Mol Biol Cell *26*, 2885-2894.
Silver, P. (2009). Indirect immunofluorescence labeling in the yeast Saccharomyces cerevisiae. Cold Spring Harb Protoc *2009*, pdb prot5317.
Taylor, S.D., Zhang, H., Eaton, J.S., Rodeheffer, M.S., Lebedeva, M.A., O'Rourke T, W., Siede, W., and Shadel, G.S. (2005). The conserved Mec1/Rad53 nuclear checkpoint pathway regulates mitochondrial DNA copy number in Saccharomyces cerevisiae. Mol Biol Cell *16*, 3010-3018.
Traven, A., Janicke, A., Harrison, P., Swaminathan, A., Seemann, T., and Beilharz, T.H. (2012). Transcriptional profiling of a yeast colony provides new insight into the heterogeneity of multicellular fungal communities. PLoS One *7*, e46243.
Ulery, T.L., Jang, S.H., and Jaehning, J.A. (1994). Glucose repression of yeast mitochondrial transcription: kinetics of derepression and role of nuclear genes. Mol Cell Biol *14*, 1160-1170.
Venkatesh, S., Lee, J., Singh, K., Lee, I., and Suzuki, C.K. (2012). Multitasking in the mitochondrion by the ATP-dependent Lon protease. Biochim Biophys Acta *1823*, 56-66.
Wei, J., and Sherman, F. (2004). Sue1p is required for degradation of labile forms of altered cytochromes C in yeast mitochondria. The Journal of biological chemistry *279*, 30449-30458.
Williams, R.S. (1986). Mitochondrial gene expression in mammalian striated muscle. Evidence that variation in gene dosage is the major regulatory event. The Journal of biological chemistry *261*, 12390-12394.
Yen, J.C., Chang, F.J., and Chang, S. (1995). A new criterion for automatic multilevel thresholding. IEEE Trans Image Process *4*, 370-378.
Ylikallio, E., Tyynismaa, H., Tsutsui, H., Ide, T., and Suomalainen, A. (2010). High mitochondrial DNA copy number has detrimental effects in mice. Hum Mol Genet *19*, 2695-2705.
Yu, M. (2011). Generation, function and diagnostic value of mitochondrial DNA copy number alterations in human cancers. Life Sci *89*, 65-71.
Zelenaya-Troitskaya, O., Newman, S.M., Okamoto, K., Perlman, P.S., and Butow, R.A. (1998). Functions of the high mobility group protein, Abf2p, in mitochondrial DNA segregation, recombination and copy number in Saccharomyces cerevisiae. Genetics *148*, 1763-1776.
Zhang, H., and Singh, K.K. (2014). Global genetic determinants of mitochondrial DNA copy number. PLoS One *9*, e105242.

912 **Figure Legends**

913 **Figure 1:** A forward genetic screen to identify cellular machineries regulating mtDNA copy
914 number.

915 A) Schematic illustration of the genetic screen. Mutants of the yeast deletion library were grown
916 on agar plates (fermentable rich media, YPD) and transferred to nylon membranes (1), lysed
917 and hybridized with two sets of fluorescent probes specific for mitochondrial DNA (green) or
918 nuclear DNA (red) (2).

919 B) Scan of a colony blot is shown as overlay of two channels. Each mutant has its replicate on
920 the diagonal. Mutants with mtDNA/nDNA ratios similar to WT appear yellow; whereas mutants
921 with increased or decreased mtDNA levels are depicted in green and red, respectively.

922 C) Histogram showing distribution of relative fold changes in mtDNA/nDNA ratios of the
923 mutants. Error bars indicate standard deviations (SD) of three independent colony blot
924 experiments (n=3). 2.4% of total mutants showed an increase in mtDNA copy number by at
925 least 50% (green). 3.5% of total mutants lost the majority of or lack mtDNA (red).
926 mtDNA/nDNA ratios below zero is due to subtraction of colony auto-fluorescence from
927 hybridization signal (Supp. Fig. 1; for the list of mutants see Supp. Table 1).

928 D) mtDNA levels of 91 hits identified by colony blot screens, were verified by qPCR, shown as
929 an average of two independent experiments. Cell sizes of mutants were determined by flow
930 cytometry using SSC-H. Values are relative to WT (see Supp. Table 1D). Three mutants
931 showing budding defects were omitted from analysis; WT shown in black. Dashed line marks
932 10% cut off. Cells were grown in YPD.

933 E) The list of genes identified in this study; their deletion mutants lead to an increase in mtDNA
934 copy number but their cell size remained within 10% change of WT. mtDNA levels and cell

935 sizes were determined relative to WT (n=2).

Figure 2: Deletion of an uncharacterized gene, *MRX6*, increases mtDNA copy number.

A) qPCR analyses of mtDNA copy number in haploid and diploid W303 cells lacking *MRX6.* Cells were grown in YPD. Error bars indicate SD (n=4).

B) Growth curves of WT and Δ*mrx6* cells grown in YPD or YPEG (rich media with ethanol and glycerol). (n=2).

C) qPCR analyses of mtDNA levels in WT and Δ*mrx6* cells grown in YPD, YPEG or treated with 0.5mM H_2O_2 in YPD for one hour. (YPD and YPD+ H_2O_2, n=2; YPEG, n=4).

D) qPCR analyses of mtDNA levels in WT and Δ*mrx6* cells grown in YPD and treated with DMSO or FCCP (5μg/ml) for one hour. (n=2).

E) Western Blot analyses of Mrx6-myc levels in cells that either express Mrx6-myc or lack Mrx6, transformed with an empty vector or a vector allowing overexpression of Mrx6–myc from the ADH1 promoter. Cells were grown in drop-out synthetic media with dextrose, lacking URA (SD-ura). PGK1 was used as a loading control.

F) qPCR analysis of mtDNA copy number in cells over-expressing Mrx6–myc, shown in Fig. 2E. (n=4).

Figure 3: Deletion of *MRX6* increases mtDNA copy number without altering mitochondrial network length and morphology.

A) Z-projections of SI microscopic images of paraformaldehyde-fixed diploid WT and Δ*mrx6* cells. Mitochondria were visualized by mitochondria-targeted dsRed protein (mt-dsRed). LacI-GFP marks mtDNA. Cells were grown in SD-ura-trp.

B, C, D, E) Number of end points (B), branch points (C), length of mitochondrial network (D) and mtDNA copy number normalized to mitochondrial network length (E) in WT and Δ*mrx6* cells. Analysis was performed on three-dimensional images (58 cells for WT, 69 cells for Δ*mrx6*).

F) Histogram showing distribution of distances between neighboring mtDNA copies in WT and Δ*mrx6* cells in three-dimensional images. Means of distance between mtDNA copies 692 nm and 872 nm for Δ*mrx6* and WT cells, respectively ($p<0.001$).

G) Histogram depicting the differences in the abundance of distances between neighboring mtDNA copies (binning range 0.1 µm) between the observed WT distribution (n=1677) and a remodeled Δ*mrx6* distribution. In the remodeled Δ*mrx6* distribution all determined distances in mutant cells (n=1677) were multiplied by factor ~1.28 assuming that distances would be only shifted linearly to closer distances in Δ*mrx6* cells compared to WT. Numbers of neighboring mtDNA copies in each binned distance range in the remodeled Δ*mrx6* distribution were substituted by the respective amount determined for the WT distribution. The distance range from 0 to 0.7 µm that is overrepresented in the remodeled Δ*mrx6* distribution is highlighted in yellow, the one underrepresented between 0.5 and 1 µm is highlighted in blue. The remodeled Δ*mrx6* distribution is significantly different from the WT distribution ($\chi^2 = 52{,}67$, df=29, $p<0.005$).

Figure 4: Δ*mrx*6 cells display elongated nucleoids.

A) Z-projections of SI microscopic images of paraformaldehyde and methanol-fixed diploid cells that were stained with DAPI. Mitochondria were visualized by mt-dsRED. Cells were grown in SD-ura-trp.

B) Number and C) average volume of nucleoids stained with DAPI in WT and Δ*mrx6* cells. Analysis was performed on three-dimensional images. (31 cells for WT, 47 cells for Δ*mrx6*)

Figure 5: Mrx6 is a member of the PET20 domain-containing protein family.

A) Domain architecture of Mrx6 and other PET20 domain-containing proteins. Blue indicates mitochondrial targeting sequences. Orange represents PET20 domain.

B) Analysis of mtDNA copy number of single, double and triple deletion mutants of *MRX6, PET20* and *SUE1,* measured by qPCR. Error bars are SD (n=2). Cells were grown in YPD.

Figure 6: Mrx6 forms foci in mitochondria and colocalizes with mtDNA.

A) Z-projection of microscopic images of a live cell expressing Mrx6-Neon. Mitochondria were visualized by mt-BFP. Mrx6-Neon (green), mt-BFP (blue) in the merged image. Cells were grown in SD-ura-trp.

B) Z-projections of microscopic images of a live cell expressing Mrx6-Neon (green). mtDNA was stained with DAPI (blue). Arrowhead shows colocalization of Mrx6-Neon and DAPI; asterisk marks non-colocalization. Cells were grown in SD-trp.

C) Line scan analysis of mitochondrial network for the cell shown in Fig. 6B.

D) Distribution of Manders' Colocalization Coefficients (MCC) calculated for colocalization of Mrx6-Neon with DAPI in 47 cells (mean=0.60) or in same line scans where the DAPI signal was randomized (mean=0.42, $p<0.001$).

E) Distribution of Pearson's Correlation Coefficients (PCC) determined for Mrx6-Neon and DAPI line scans in measured data (n=47 cells, mean=0.40) and in randomized data (mean=0, p= $p<0.001$).

F) Z-projection of microscopic images of a live cell that lacks mtDNA but expresses Mrx6-Neon (green). Mitochondria were visualized by mt-BFP (blue). Cells were grown in SD-ura.

Figure 7: Mrx6 binds to Pet20, Pim1 and Mam33.

A) Western Blot analyses of an anti-Flag immunoprecipitation experiment from cells expressing Mrx6-Flag or Mrx6 (WT). Membranes were probed with antibodies against Pim1 (top) and the Flag-epitope (bottom). Cells were grown in YPD.

B) Interaction partners of Mrx6-Flag in cells expressing Mrx6-Flag; expressing Mrx6-Flag but lacking Pet20 or Sue1, identified by anti-Flag immunoprecipitations and mass spectrometry analyses. The numbers represent total spectral count. Cells were grown in YPD.

C) Interaction partners of Pet20-Flag in cells expressing Pet20-Flag; expressing Pet20-Flag but lacking Mrx6 or Sue1. Same as above.

D) Interaction partners of Sue1-Flag in cells expressing Sue1-Flag; expressing Sue1-Flag but lacking Mrx6 or Pet20. Same as above.

Figure 8: Mrx6 partially colocalizes with Pet20 and Pim1.

A) Z-projections of microscopic images of a live cell expressing Mrx6-Neon (green), and Pet20-Ruby (red). Line scan analysis of mitochondrial network is shown on the right. Arrowhead indicates colocalization of Mrx6-Neon and Pet20-Ruby; asterisk marks non-colocalization. Cells were grown in SD-ura-trp.

B) Distribution of Manders' Colocalization Coefficients (MCC) determined for colocalization of Mrx6-Neon with Pet20-Ruby in measured (n=41 cells, mean=0.50) and randomized data (mean=0.36, $p<0.001$).

C) Distribution of Pearson's Correlation Coefficients (PCC) between Mrx6-Neon and Pet20-Ruby in measured (n=41 cells, mean=0.28) and randomized data (mean=0, $p<0.001$).

D) Z-projections of microscopic images of a live cell expressing Mrx6-Neon (green), and Pim1-Ruby (red). Line scan analysis of mitochondrial network is shown on the right. Arrowhead indicates colocalization of Mrx6-Neon and Pim1-Ruby; asterisk marks non-colocalization. Cells were grown in SD-ura-trp.

E) Distribution of Manders' Colocalization Coefficients (MCC) determined for colocalization of Mrx6-Neon with Pim1-Ruby in measured (n=69 cells, mean=0.50) and randomized data (mean=0.37, $p<0.001$).

F) Distribution of Pearson's Correlation Coefficients (PCC) between Mrx6-Neon and Pim1-Ruby in measured (n=69 cells, mean=0.22) and randomized data (mean=0, $p<0.001$).

Figure 9: Mrx6 colocalizes with Pet20 and Pim1 in regions close to mtDNA.

A) Z-projections of microscopic images of a live cell expressing Mrx6-Neon and Pet20-Ruby. mtDNA was stained with DAPI. Mrx6-Neon (green), Pet20-Ruby (red), and DAPI (blue) in the merged images. Line scan analysis of mitochondrial network is shown on the right. Arrowhead indicates colocalization of Mrx6-Neon, Pet20-Ruby and DAPI signal. Cells were grown in SD-trp.

B) Distribution of Manders' Colocalization Coefficients (MCC) determined for colocalization of Mrx6-Pet20 (Mrx6-Neon colocalizing with Pet20-Ruby) with DAPI signal (n=25 cells, mean=0.77); and Mrx6 alone (not colocalizing with Pet20-Ruby) with DAPI signal (mean=0.56, $p<0.001$).

C) Distribution of Manders' Colocalization Coefficients (MCC) determined for colocalization of Mrx6-Pet20 (Mrx6-Neon colocalizing with Pet20-Ruby) with randomized DAPI signal (n=25 cells, mean=0.44); and Mrx6-Neon alone (not colocalizing with Pet20-Ruby) with randomized DAPI signal (mean=0.45, $p=0.78$).

D) Z-projections of microscopic images of a live cell expressing Mrx6-Neon (green) and Pim1-Ruby (red). mtDNA was stained with DAPI (blue). Line scan analysis of mitochondrial network is shown on the right. Arrowhead indicates colocalization of Mrx6-Neon, Pim1-Ruby and DAPI signal. Cells were grown in SD-trp.

E) Distribution of Manders' Colocalization Coefficients (MCC) determined for colocalization of Mrx6-Pim1 (Mrx6-Neon colocalizing with Pim1-Ruby) with DAPI signal (n=49 cells, mean=0.65) and Mrx6 alone (not colocalizing with Pim1-Ruby) with DAPI signal (mean=0.46, $p<0.001$).

F) Distribution of Manders' Colocalization Coefficient (MCC) determined for colocalization of Mrx6-Pim1 (Mrx6-Neon colocalizing with Pim1-Ruby) with randomized DAPI signal (n=49 cells, mean=0.38); and Mrx6 alone (not colocalizing with Pim1-Ruby) with randomized DAPI signal (mean=0.37, p=0.49).

Figure 10: Acute depletion of Pim1 results in increased mtDNA copy number similar to levels of Δ*mrx6* cells but does not further exceed these levels in the double mutant.

A) qPCR analyses of mtDNA copy number in cells that harbor an estradiol inducible Pim1 expression construct and lack either only *PIM1* (Δ*pim1 Pestr*-PIM1) or both *PIM1* and *MRX6* (Δ*mrx6* Δ*pim1 Pestr*-PIM1). 25nM estradiol was supplied for Pim1 expression and omitting estradiol from the medium induced acute depletion of Pim1. Cells were continuously maintained at log-phase in SC medium and harvested at OD_{600}=1 at the respective time points for DNA extraction. (n=3 with 3 technical replicates each).

B) Western Blot analyses of Pim1 levels in estradiol regulatable strains and WT. The cells harvested for Fig. 10A were used for this experiment as well.

C) Drop dilution growth analysis of estradiol inducible Pim1 strains in comparison to WT and Δ*pim1*. The 11200 cells were serially diluted at a ratio of 1:5 and the dilutions were spotted on fermentable (SC-medium) and non-fermentable carbon sources (YPG-medium) supplemented with 25 nM estradiol or not, and cultivated for 2 days at 30 °C.

Figure 11: Model for the role of the Mrx6 complex in mtDNA replication.

(A) The Mrx6 complex colocalizes preferentially with mtDNA, whereas single components are more often found in areas that lack mtDNA. (B) Mrx6 is essential for the formation of a Pim1 containing complex that controls mtDNA levels, whereas Pet20 is dispensable for sufficient mtDNA copy number control. (C) We propose that Mrx6 may facilitate substrate recognition of Pim1 and degradation of replication factors (RF) that stimulate mtDNA replication. Accordingly, absence of Mrx6 would lead to accumulation of such factors and result in increased amounts of mtDNA.

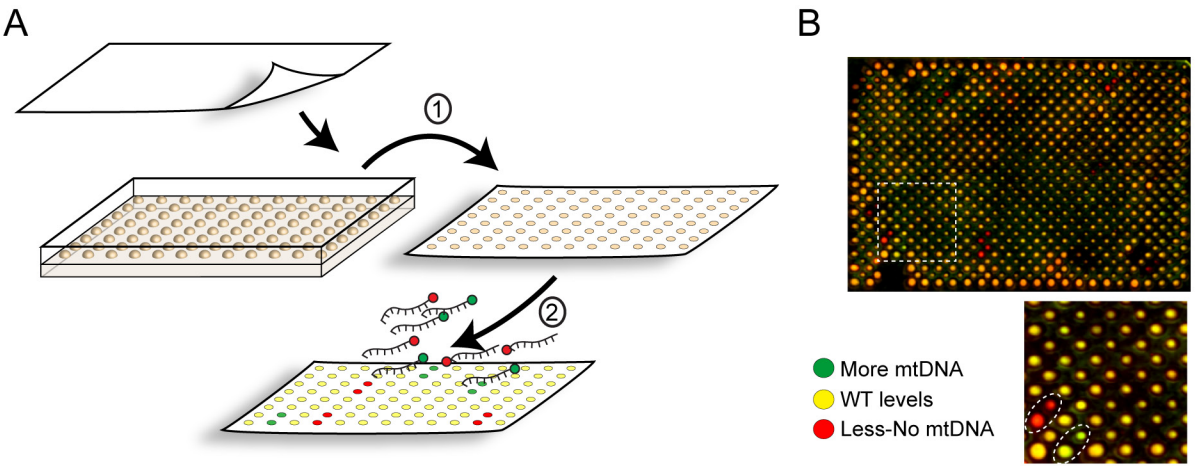

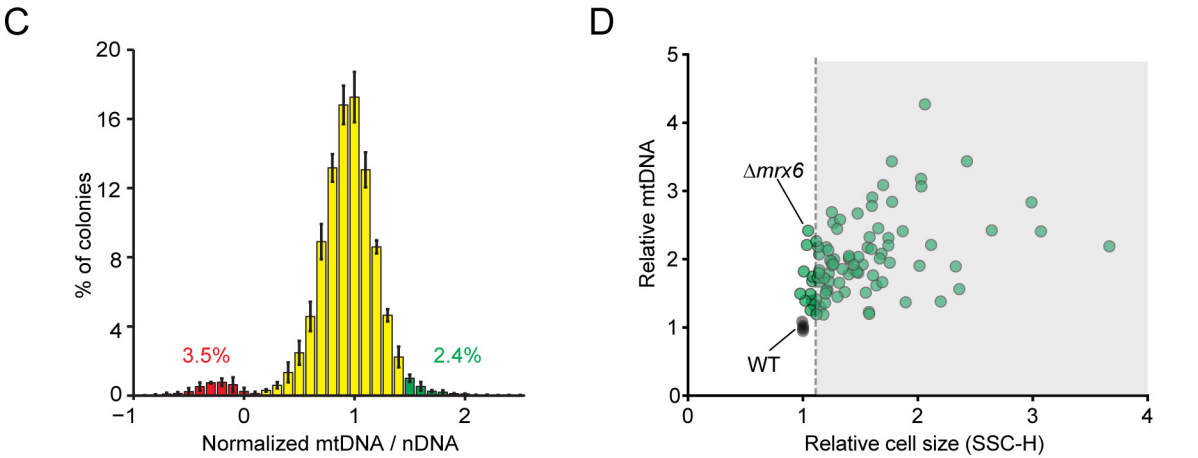

E

Gene ID	Gene name	Relative mtDNA (qPCR)	SEM (qPCR)	Relative cell size (SSC-H)	SEM (SSC-H)
YNL295W	*MRX6*	2.42	0.13	1.05	0.00
YOL076W	*MDM20*	2.26	0.22	1.12	0.07
YOR114W	*YOR114W*	2.21	0.39	1.03	0.01
YDR448W	*ADA2*	1.82	0.07	1.01	0.04
YLR176C	*RFX1*	1.74	0.06	1.09	0.01
YDL049C	*KNH1*	1.68	0.09	1.08	0.01
YGR252W	*GCN5*	1.50	0.08	0.98	0.07
YMR100W	*MUB1*	1.49	0.27	1.07	0.00
YBR194W	*AIM4*	1.39	0.09	1.02	0.01

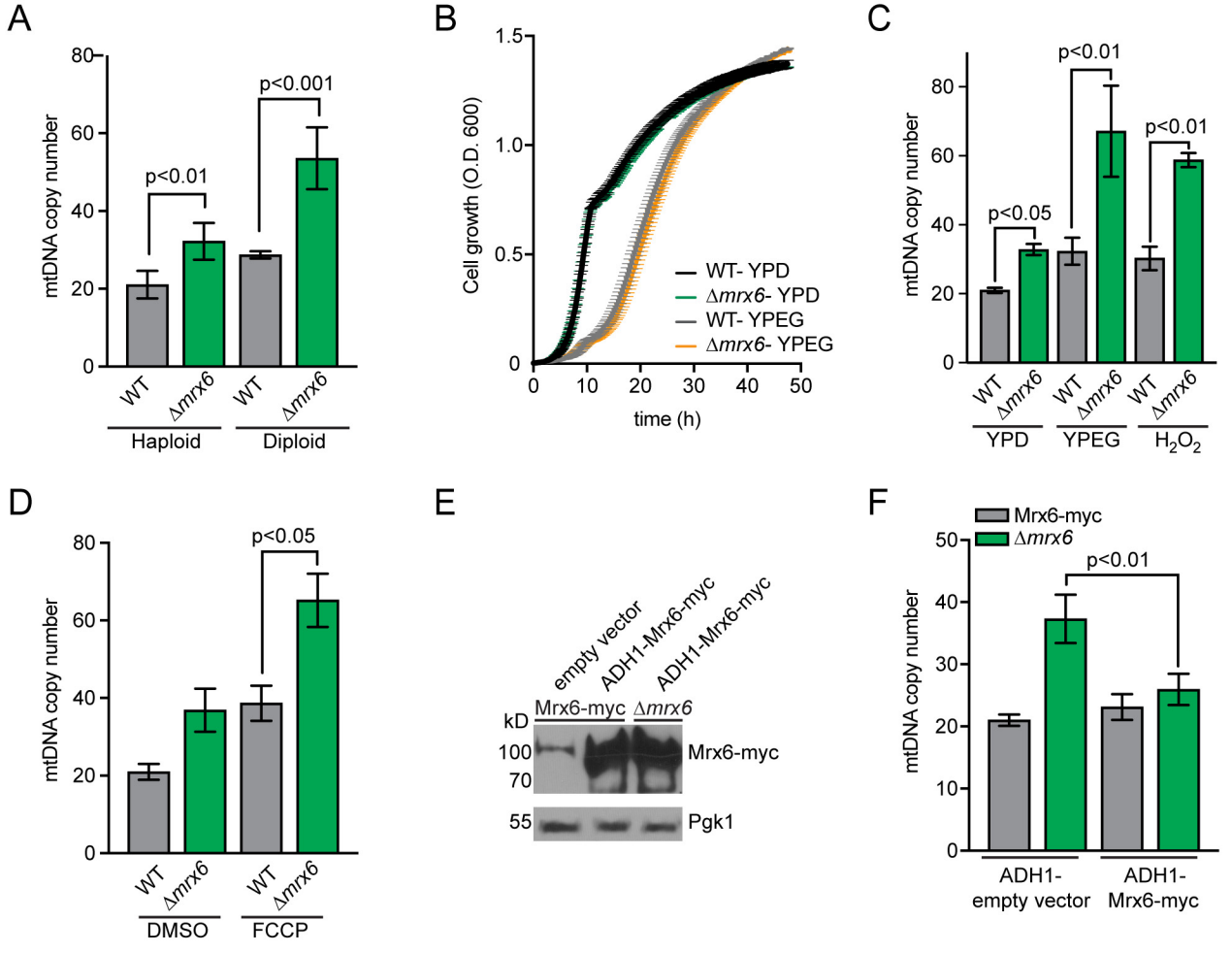
A
mtDNA copy number
p<0.01
p<0.001
WT
Δmrx6
WT
Δmrx6
Haploid
Diploid
B
Cell growth (O.D. 600)
time (h)
WT- YPD
Δmrx6- YPD
WT- YPEG
Δmrx6- YPEG
C
mtDNA copy number
p<0.05
p<0.01
p<0.01
YPD
YPEG
H2O2
D
mtDNA copy number
p<0.05
DMSO
FCCP
E
empty vector
ADH1-Mrx6-myc
ADH1-Mrx6-myc
kD
Mrx6-myc
Δmrx6
100
70
Mrx6-myc
55
Pgk1
F
Mrx6-myc
Δmrx6
mtDNA copy number
p<0.01
ADH1-
empty vector
ADH1-
Mrx6-myc

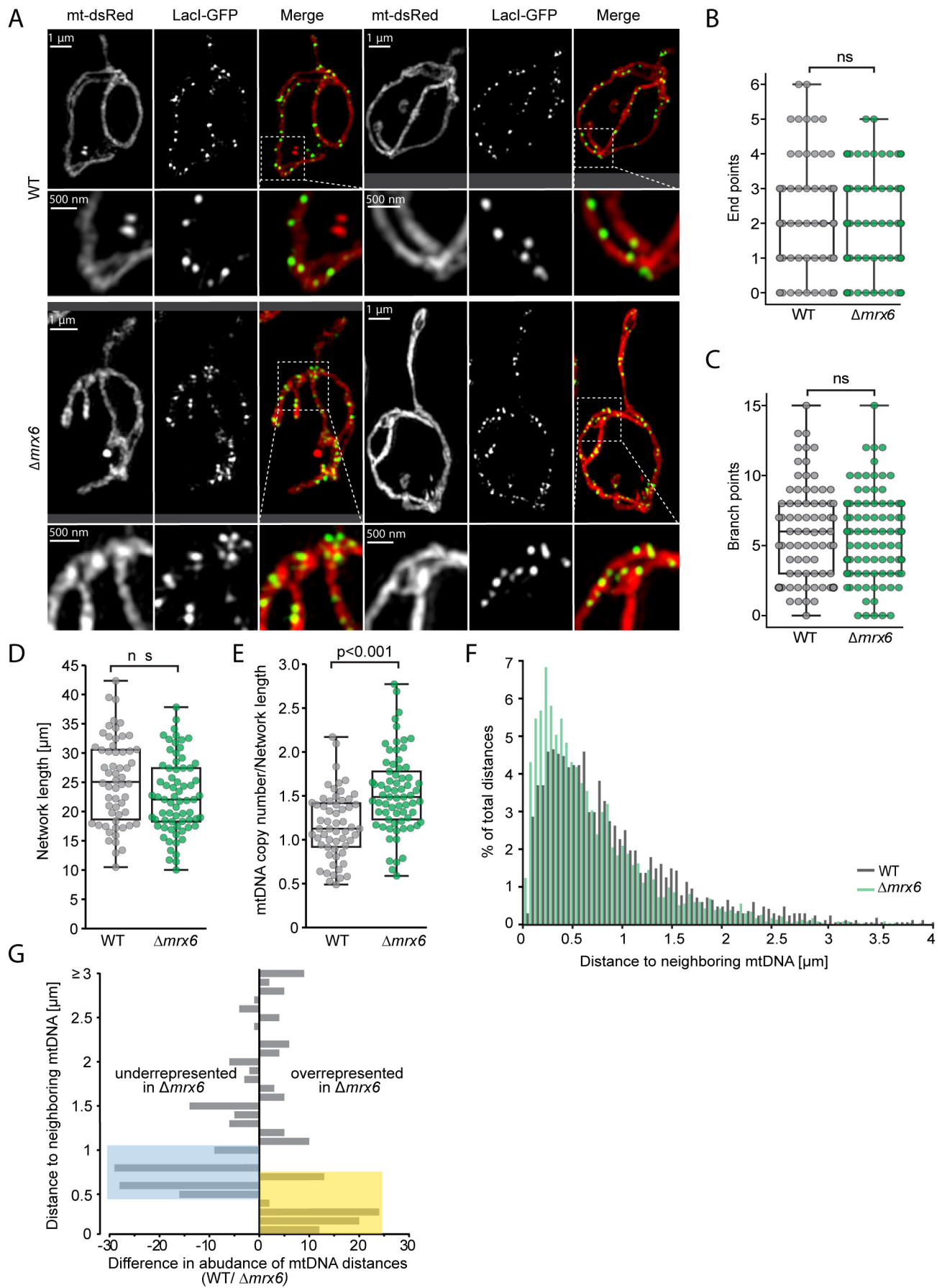
A
mt-dsRed
LacI-GFP
Merge
mt-dsRed
LacI-GFP
Merge
WT
Δmrx6
1 µm
500 nm
B
ns
End points
WT
Δmrx6
C
ns
Branch points
WT
Δmrx6
D
n s
Network length [µm]
WT
Δmrx6
E
p<0.001
mtDNA copy number/Network length
WT
Δmrx6
F
% of total distances
WT
Δmrx6
Distance to neighboring mtDNA [µm]
G
Distance to neighboring mtDNA [µm]
underrepresented in Δmrx6
overrepresented in Δmrx6
Difference in abudance of mtDNA distances (WT/ Δmrx6)

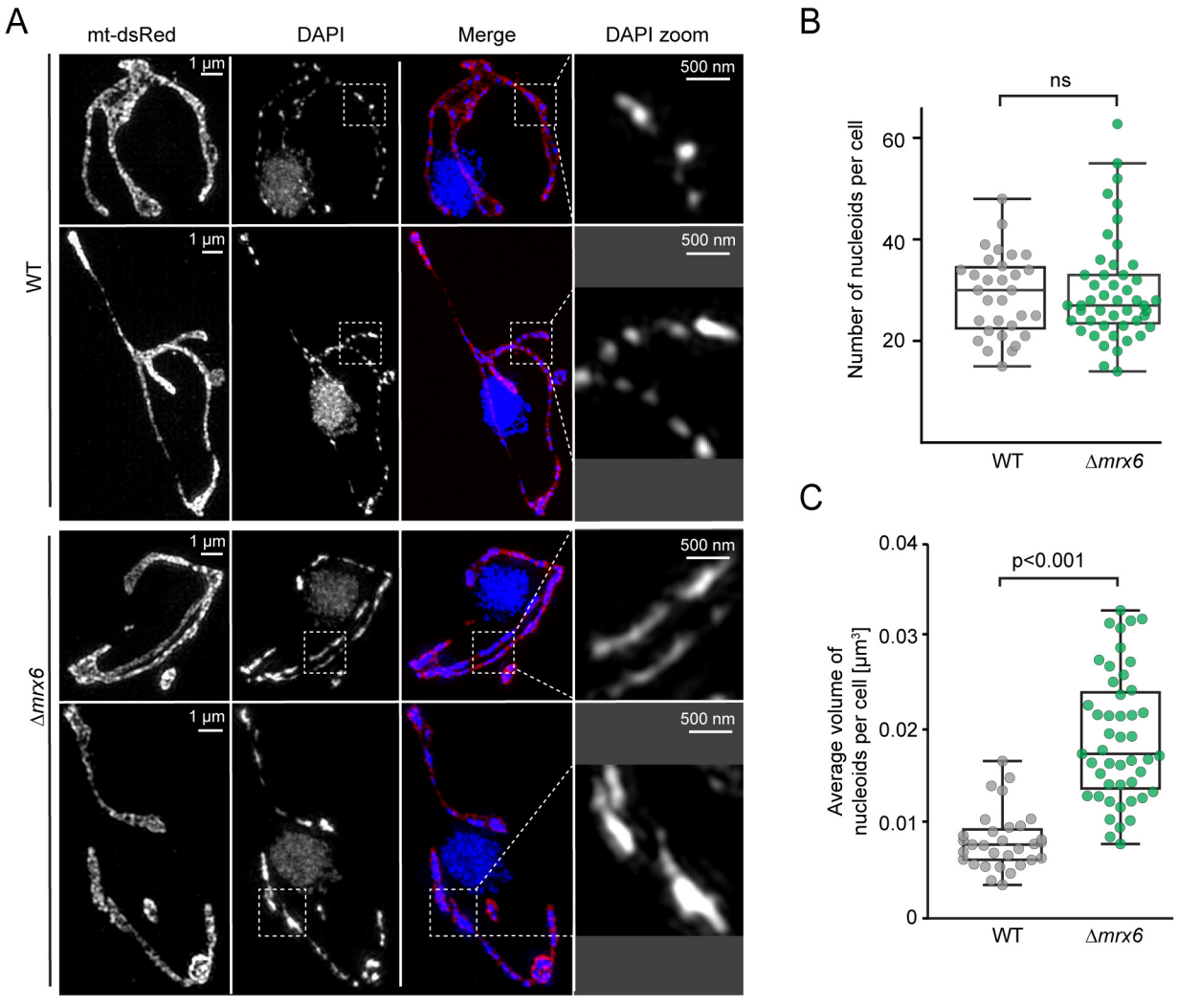
A
mt-dsRed
DAPI
Merge
DAPI zoom
WT
Δmrx6
1 µm
500 nm
B
ns
Number of nucleoids per cell
60
40
20
WT
Δmrx6
C
p<0.001
Average volume of nucleoids per cell [µm³]
0.04
0.03
0.02
0.01
0
WT
Δmrx6

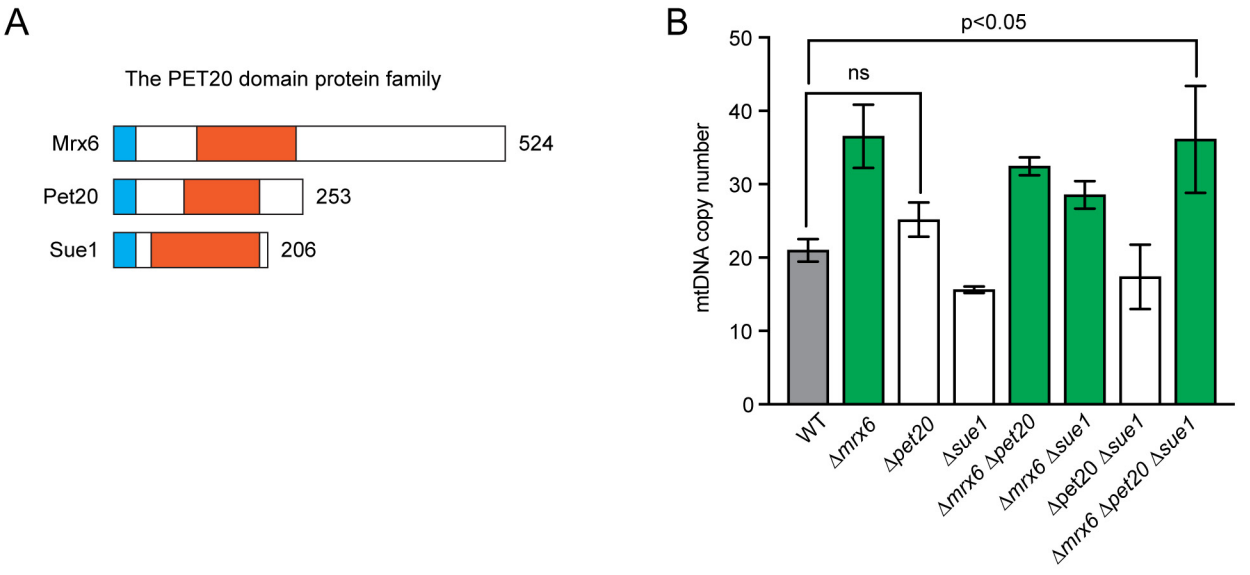
A
The PET20 domain protein family
Mrx6
524
Pet20
253
Sue1
206
B
p<0.05
ns
mtDNA copy number
50
40
30
20
10
0
WT
Δmrx6
Δpet20
Δsue1
Δmrx6 Δpet20
Δmrx6 Δsue1
Δpet20 Δsue1
Δmrx6 Δpet20 Δsue1

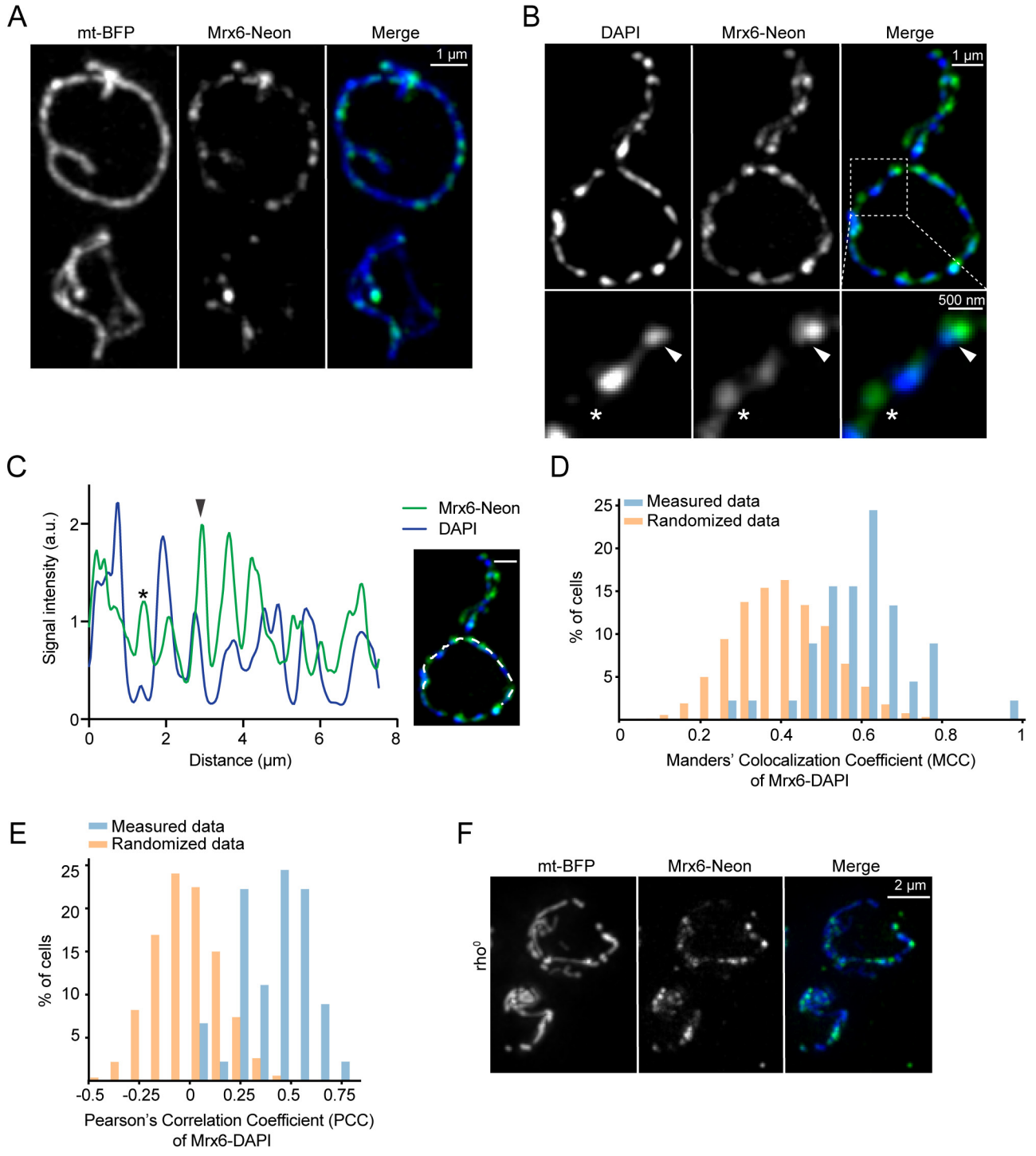
A
mt-BFP
Mrx6-Neon
Merge
1 µm
B
DAPI
Mrx6-Neon
Merge
1 µm
500 nm
C
Signal intensity (a.u.)
Distance (µm)
Mrx6-Neon
DAPI
D
Measured data
Randomized data
% of cells
Manders' Colocalization Coefficient (MCC) of Mrx6-DAPI
E
Measured data
Randomized data
% of cells
Pearson's Correlation Coefficient (PCC) of Mrx6-DAPI
F
mt-BFP
Mrx6-Neon
Merge
2 µm
rho0

A

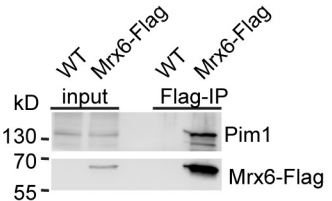

B

Mrx6-Flag immunoprecipitation

	WT	Mrx6-Flag	Δ*pet20* Mrx6-Flag	Δ*sue1* Mrx6-Flag
Pim1	0	555	354	434
Mrx6	0	151	98	114
Pet20	0	44	0	44
Mam33	0	66	44	42

Total spectral count

C

Pet20-Flag immunoprecipitation

	WT	Pet20-Flag	Δ*mrx6* Pet20-Flag	Δ*sue1* Pet20-Flag
Pim1	0	391	6	484
Mrx6	0	67	0	86
Pet20	0	50	21	67
Mam33	0	39	0	46

Total spectral count

D

Sue1-Flag immunoprecipitation

	WT	Sue1-Flag	Δ*pet20* Sue1-Flag	Δ*mrx6* Sue1-Flag
Pim1	0	59	55	41
Mrx6	0	0	0	0
Pet20	0	0	0	0
Mam33	0	0	0	0
Sue1	0	3	4	3

Total spectral count

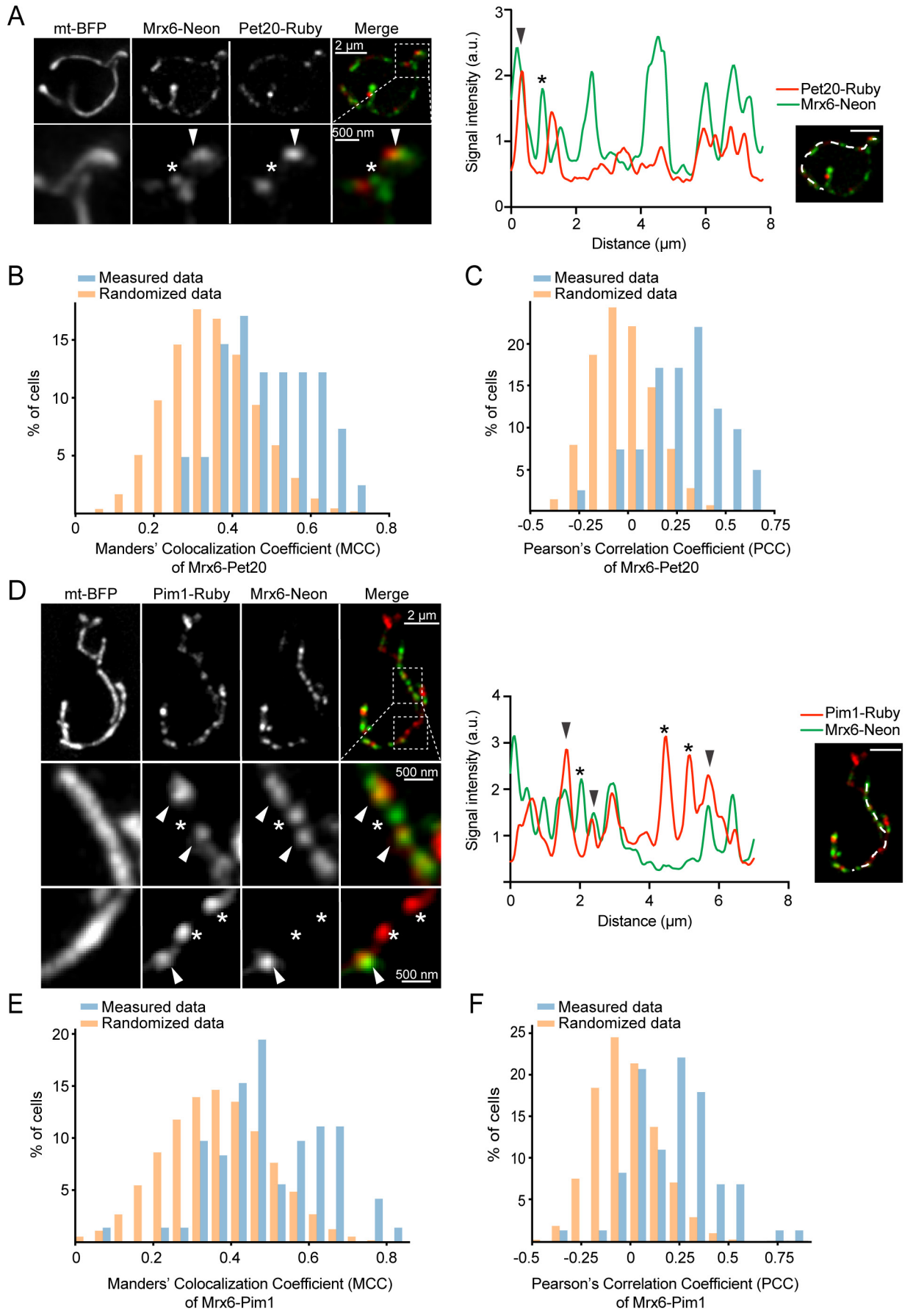
A
mt-BFP
Mrx6-Neon
Pet20-Ruby
Merge
2 μm
500 nm
Signal intensity (a.u.)
Distance (μm)
Pet20-Ruby
Mrx6-Neon
B
Measured data
Randomized data
% of cells
Manders' Colocalization Coefficient (MCC)
of Mrx6-Pet20
C
Measured data
Randomized data
% of cells
Pearson's Correlation Coefficient (PCC)
of Mrx6-Pet20
D
mt-BFP
Pim1-Ruby
Mrx6-Neon
Merge
2 μm
500 nm
Signal intensity (a.u.)
Distance (μm)
Pim1-Ruby
Mrx6-Neon
E
Measured data
Randomized data
% of cells
Manders' Colocalization Coefficient (MCC)
of Mrx6-Pim1
F
Measured data
Randomized data
% of cells
Pearson's Correlation Coefficient (PCC)
of Mrx6-Pim1

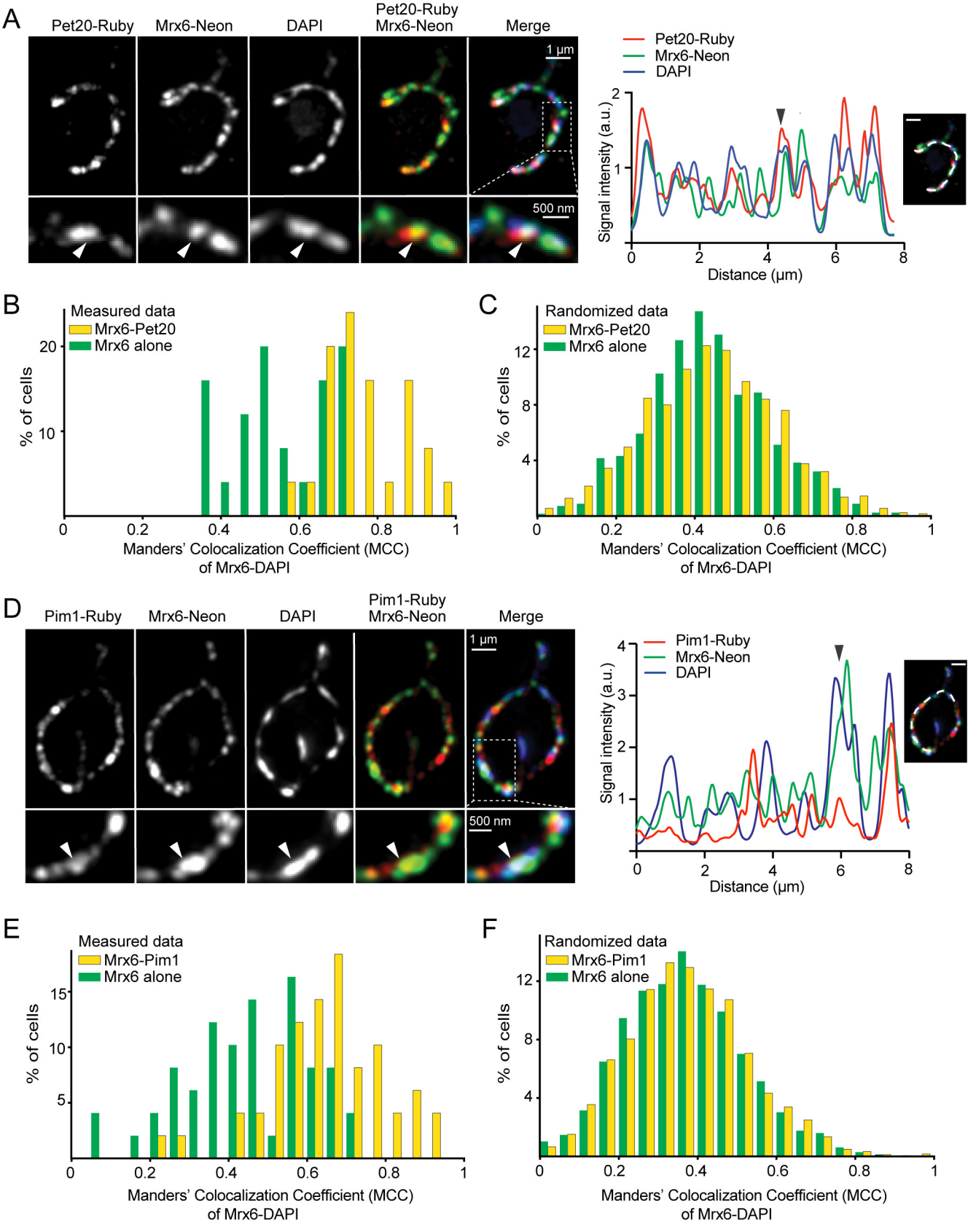
A
Pet20-Ruby
Mrx6-Neon
DAPI
Pet20-Ruby
Mrx6-Neon
Merge
1 µm
500 nm
Pet20-Ruby
Mrx6-Neon
DAPI
Signal intensity (a.u.)
Distance (µm)
B
Measured data
Mrx6-Pet20
Mrx6 alone
% of cells
Manders' Colocalization Coefficient (MCC)
of Mrx6-DAPI
C
Randomized data
Mrx6-Pet20
Mrx6 alone
% of cells
Manders' Colocalization Coefficient (MCC)
of Mrx6-DAPI
D
Pim1-Ruby
Mrx6-Neon
DAPI
Pim1-Ruby
Mrx6-Neon
Merge
1 µm
500 nm
Pim1-Ruby
Mrx6-Neon
DAPI
Signal intensity (a.u.)
Distance (µm)
E
Measured data
Mrx6-Pim1
Mrx6 alone
% of cells
Manders' Colocalization Coefficient (MCC)
of Mrx6-DAPI
F
Randomized data
Mrx6-Pim1
Mrx6 alone
% of cells
Manders' Colocalization Coefficient (MCC)
of Mrx6-DAPI

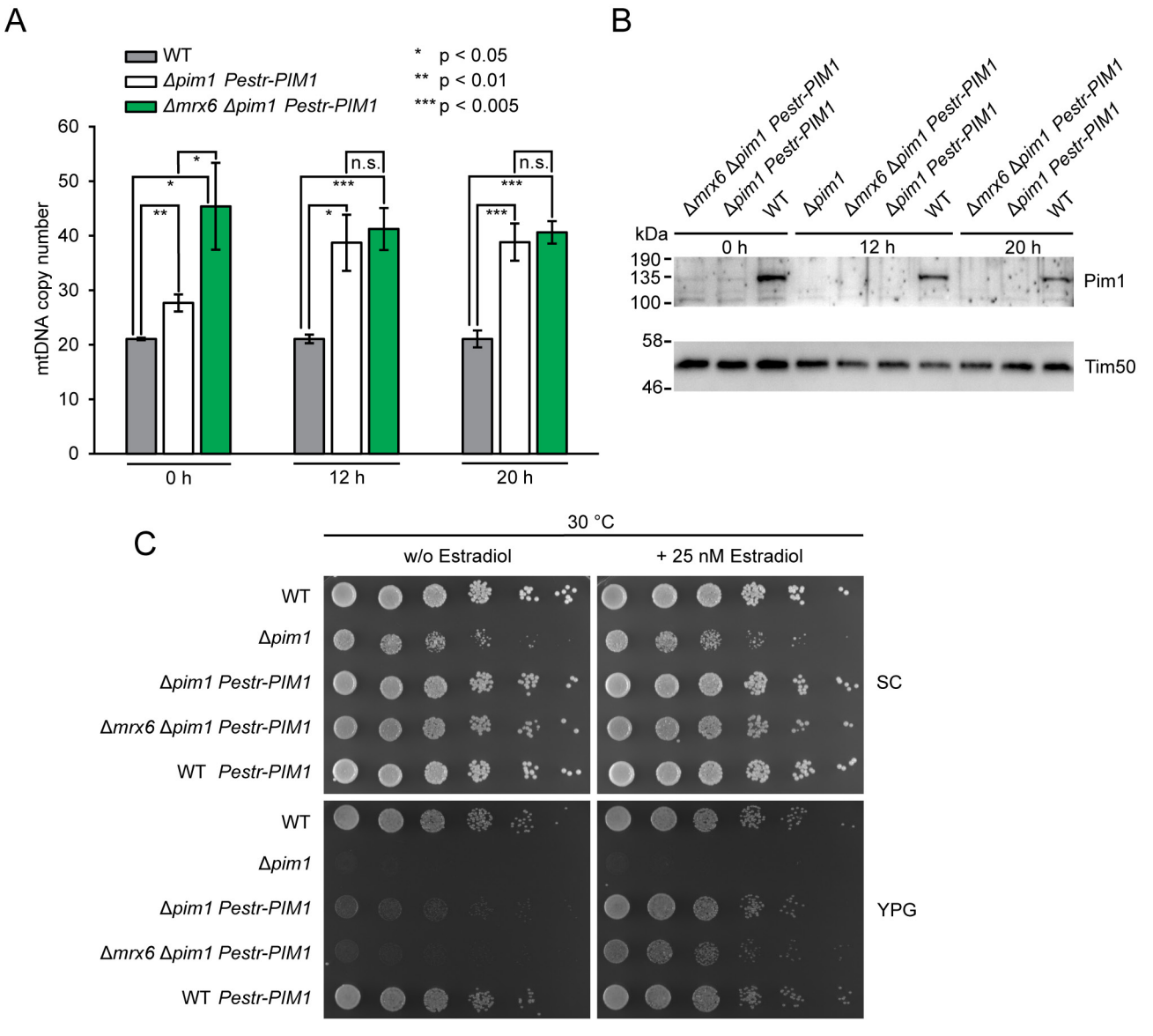
A
WT
Δpim1 Pestr-PIM1
Δmrx6 Δpim1 Pestr-PIM1
* p < 0.05
** p < 0.01
*** p < 0.005
mtDNA copy number
0 h
12 h
20 h
n.s.
B
Δmrx6 Δpim1 Pestr-PIM1
Δpim1 Pestr-PIM1
WT
Δpim1
kDa
0 h
12 h
20 h
190
135
100
58
46
Pim1
Tim50
C
30 °C
w/o Estradiol
+ 25 nM Estradiol
WT
Δpim1
Δpim1 Pestr-PIM1
Δmrx6 Δpim1 Pestr-PIM1
WT Pestr-PIM1
SC
YPG

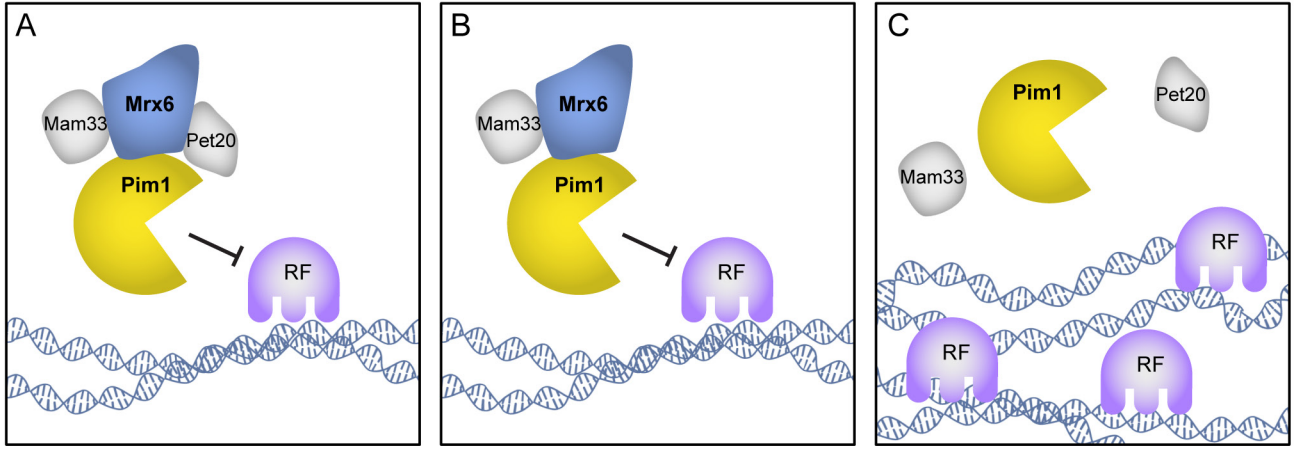

mtDNA amount is controlled

mtDNA amount is controlled

mtDNA amount is increased